Title
Lidar Boosts 3D Ecological Observations and Modeling

Journal
IEEE Geoscience and Remote Sensing Magazine, 9(1)

ISSN
2473-2397

Authors
Guo, Qinghua
Su, Yanjun
Hu, Tianyu
et al.

Publication Date
2021-03-01

DOI
10.1109/mgrs.2020.3032713

Peer reviewed

Lidar Boosts 3D Ecological Observations and Modeling

A review and perspective

QINGHUA GUO, YANJUN SU, TIANYU HU, HONGCAN GUAN, SHICHAO JIN, JING ZHANG, XIAOXIA ZHAO, KEXIN XU, DENGJIE WEI, MAGGI KELLY, AND NICHOLAS C. COOPS

The advent of lidar has revolutionized the way we observe and measure vegetation structure from the ground and from above and represents a major advance toward the quantification of 3D ecological observations. Developments in lidar hardware systems and data processing algorithms have greatly improved the accessibility and ease of use of lidar observations in ecological studies. A wide range of studies has been devoted to accurately measuring and modeling vegetation structural and functional attributes from lidar data across a range of spatial scales (from individual organs to global scales) and ecosystem types (e.g., forest, agricultural, grassland, and urban ecosystems).

As lidar technologies and applications advance, there is an increasing recognition of the importance of studying 3D ecosystem structures. Research has demonstrated that lidar observations can be effectively used to calibrate and improve ecological models and produce more detailed and accurate results, bringing new ecological insights that challenge our existing knowledge. Nevertheless, we argue that the incorporation of 3D lidar observations into ecological models remains in its infancy, and the potential of fusing 3D lidar observations with multisource remote sensing data for contributing to a new understanding of ecological processes has not yet been fully explored. The acquisition of 3D ecological observations should continue embracing the era of multidimensional big remote sensing data, bringing both new challenges and opportunities. Exploring the potential of multitemporal and multiplatform remote sensing data through data fusion will benefit the next generation of ecological models.

Digital Object Identifier 10.1109/MGRS.2020.3032713
Date of current version: 24 December 2020

OVERVIEW

Remote sensing has been recognized as an effective technique for describing and analyzing the status of ecosystems from individual plots to the entire biosphere [1], [2]. Data sets acquired by near-surface, airborne, and spaceborne platforms are widely used by ecologists to characterize and model ecosystem processes and to understand the fundamental theories that shape our ecosystems [3], [4]. The accumulation of time-series remotely sensed imagery from the Landsat set of sensors, the Sentinel set of sensors, and Moderate-Resolution Imaging Spectrometer (MODIS) further advances our capability to monitor ecosystem changes and predict their responses to the changing climate [5]–[8]. Using this type of optical, passive remotely sensed data, our ecological interpretation depends upon the observed land surface reflectance, which is a function of the sun and sensor viewing geometry and of the optical attributes of the land surface objects (Figure 1) [9], [10]. When these interpretations are linked to vegetation, they are mostly limited to the canopy surface since the observed within-canopy and ground reflectance is a function of vertical plant area densities [11]. However, the vertical information and internal structure of vegetation are often neglected or represented by simple geometric models in these types of ecological studies [12], [13]. Although a wide body of work is devoted to deriving vegetation structure information from these passive optical images [14], the accuracy of the derived vegetation structural attributes has generally been

low [15], [16] and progressed slowly until the emergence of lidar technology.

Unlike optical remote sensing, which measures land surface reflectance, lidar is an active remote sensing technique that measures the distance from the sensor to targeted objects by recording the time of flight of emitted laser pulses (Figure 1). The distance measurements are then converted to accurate 3D coordinates through the aid of positioning techniques (i.e., integrated navigation algorithms and simultaneous localization and mapping algorithms) [17]–[19]. Because short-wavelength laser pulses can penetrate vegetation canopies through gaps in leaves and branches, lidar can accurately depict the internal structure of vegetation canopies and shows early potential in overcoming the aforementioned obstacles of optical remote sensing [20]–[23]. Over the last three decades, lidar has been successfully used to estimate 3D vegetation attributes [e.g., vegetation height, leaf area density (LAD), and branching architecture] from plot to global scales and from individual to group levels [24], [25], enabling progress toward tackling 3D ecological problems [26]–[28].

In this review, we highlight how the increasing use of lidar has allowed a transition of ecological observations and modeling from 2D to 3D, how lidar sheds light on understanding important ecological processes, and how lidar applications should be further developed under the new paradigm of big data.

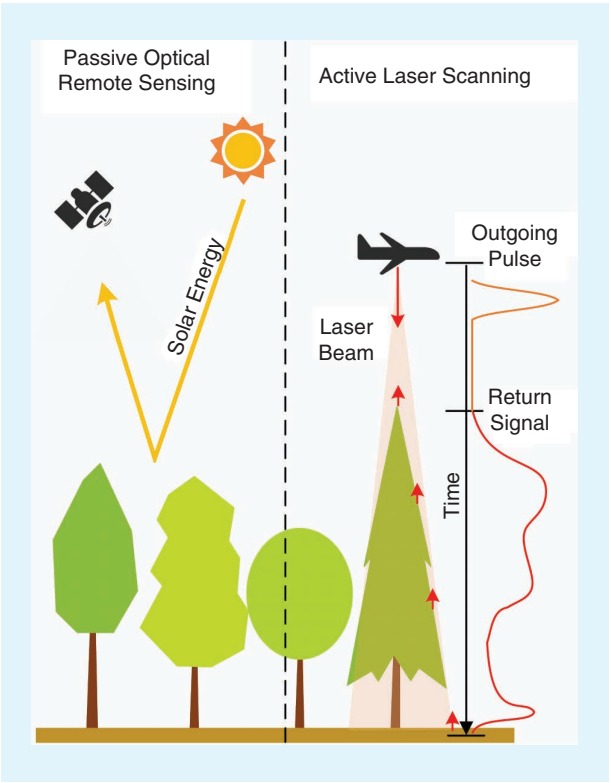

FIGURE 1. The principles of passive optical remote sensing and active laser scanning.

LIDAR DEVELOPMENT FOR ECOLOGICAL OBSERVATIONS

The increasing use and accessibility of lidar-based ecological observations can first be attributed to the development of hardware systems and data processing algorithms. On the hardware side, lidar sensors have evolved from being capable of recording only single returns per emitted pulse along a single transect [29] to recording the entire returned waveform [30]; meanwhile, the size and cost of lidar sensors has decreased significantly, greatly expanding the availability of lidar data for ecological observations. On the algorithm side, the requirement for new algorithms to deal with the complex and large-volume 3D data has introduced unprecedented challenges for the remote sensing community. Currently, we are still in the stage of developing algorithms that are robust under different topographic and vegetation conditions.

HARDWARE DEVELOPMENT

Lidar was initially designed for altimetric tasks (i.e., sea ice surface mapping and topographic mapping) using laser profiling systems [31]–[33] that recorded up to one return per emitted laser pulse [34]. Vegetation returns were usually treated as noise during this stage [33], [35]. Later, engineers equipped laser scanners with the ability to record multiple returns per emitted laser pulse and used highly precise positional information from satellite-based positioning systems, allowing the development of the basic data format of lidar, i.e., the point cloud [33], [36]. Since returns within the vegetation canopy can better describe vegetation structure, multireturn lidar represented a big leap in lidar ecological applications [37]. Further enhancing the capability of lidar in capturing vegetation structure, waveform lidar capable of recording the total amount of returned energy with a short time interval (1–5 ns, typically) emerged [30].

Laser scanners can be mounted on various types of platforms [e.g., tripods, backpacks, automobiles, unmanned aerial vehicles (UAVs), manned aircraft, and satellites], with capabilities ranging from the plot level to the global scale (Figure 2). Terrestrial laser scanners usually have a ranging limit of 100–500 m and are a desirable tool for plot-level ecological observations [38]. Although certain terrestrial laser scanners can reach a maximum range of >1 km (e.g., REIGL VZ-2000i), their use is often constrained for ecological applications due to issues of increasing sensitivity to noise in vegetated areas [39]. Traditionally, terrestrial laser scanners are mounted on fixed tripods and use a stop-and-go mode to acquire data, a method that requires a huge effort to register multiscan lidar data [40]–[42]. Recent advances in integrated navigation techniques and simultaneous localization and mapping algorithms create new possibilities to mount terrestrial laser scanners on mobile platforms, such as backpacks and ground vehicles [43], [44], greatly improving data acquisition efficiency.

Airborne lidar systems, also known as airborne laser scanning, involve the integration of positioning and

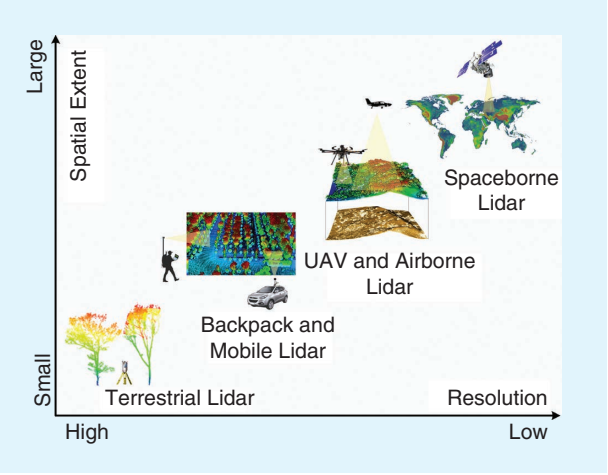

FIGURE 2. The resolution and spatial extent of various lidar platforms: terrestrial lidar, backpack and mobile lidar, unmanned aerial vehicle (UAV) and airborne lidar, and spaceborne lidar.

inertial measurement technologies and have greatly increased ranging capacity. They are often mounted on an aircraft, such as a helicopter, to cover areas ranging from hundreds to thousands of square kilometers. With the development of manufacturing technology, commercial laser scanners are becoming lighter, smaller, and cheaper. For example, solid-state lidar sensors can be lower than 1 kg in weight and less than US$1,000 in price. These sensors have greatly promoted the development of UAV lidar systems, which significantly increase the flexibility and reduce the cost of collecting landscape-scale lidar observations [45].

Spaceborne lidar systems have the longest ranging capability and are configured with a profiling design including multiple lasers. They can produce tracks or transects of laser pulses that are driven by the orbits of the platforms. For example, the footprint of the Geoscience Laser Altimeter System (GLAS) onboard the *Ice, Cloud, and Land Elevation Satellite* (*ICESat*) has a nominal diameter of ∼65 m and is separated by 170 m along track and by tens of kilometers across tracks with global coverage [46]; the footprint of the Global Ecosystem Dynamics Investigation (GEDI), launched on the International Space Station on 5 December 2018, has a nominal diameter of ∼25 m and is separated by 60 m along track and by ∼600 m across tracks and constrained between 50° S and 50° N [47]. The recent development of single-photon counting technology allows for a new mode for long-range laser scanning [48]. It uses plane array detectors to receive laser pulses with low energy and, therefore, can generate lidar data with high point density at high altitude [49]. *ICESat-2*, launched in 2018, adopted this technology to replace the waveform lidar approach of the original *ICESat* GLAS [50].

Besides the aforementioned hardware progress, recent hardware development has equipped lidar with the ability of emitting laser pulses in multiple bands (e.g., multispectral or hyperspectral lidar) [51]–[54]. This can overcome the weakness of the lack of spectral information of current lidar sensors and is beneficial for differentiating vegetation species and organs and retrieving physiological traits [55]–[57]. However, multispectral and hyperspectral sensors are still in their early developmental stages, and multispectral and hyperspectral lidar data are still very rare and expensive.

ALGORITHM DEVELOPMENT

With the continuous improvement of lidar hardware systems and the increasing availability of ground-based and aerial lidar observations, the demand for ecologically meaningful vegetation attributes from lidar observations has grown significantly. However, lidar data have required radically different data processing principles and pipelines than those provided by existing remote sensing algorithms and software.

Lidar data can be categorized into discrete lidar data and full-waveform lidar data on the basis of the data acquisition method. Discreet lidar data are most commonly distributed in the LAS format, a format specifically dedicated to storing 3D data that is standardized, documented, and maintained by the American Society for Photogrammetry and Remote Sensing. This point data format enables point cloud data to be stored optimally and contains a variety of metadata and point attributes unique to each data campaign. Accessing and processing the data from the LAS data format, however, still require a large amount of memory, necessitating the development of lidar-specific algorithms and packages to optimize processing speed and memory requirements. A range of open source and commercial applications and packages have emerged in recent years and include LiDAR360, Terrasolid Fusion, and the lidR R programming package [58], making discrete lidar data processing with user-friendly interfaces more accessible.

Compared with discrete lidar, full-waveform lidar data have the potential of detecting weak pulses [59] and providing extra waveform parameters (e.g., echo amplitude and width) [60], which have shown advantages in vegetation structure mapping and species recognition [61], [62]. However, full-waveform lidar data can be relatively difficult to interpret visually and are usually decomposed into discrete lidar data before use [63]. Decomposition processes assume that lidar waveform is a sum of Gaussian components that can be described by Gaussian functions [30]. The essential step is to discriminate the number of land surface responses from lidar waveforms and to estimate the initial parameters for waveform decomposition [64].

Several approaches have been developed to fulfill this goal, including the traditional pulse detection approach [63], the nonlinear least-squares approach using the Levenberg–Marquardt optimization algorithm [61], [65], [66], the maximum likelihood approach using an expectation–maximization algorithm [67], and the stochastic approach using the reversible jump Monte Carlo Markov chain method [68]. With the estimated initial parameters, waveform decomposition can be implemented by iteratively fitting each detected echo with a Gaussian model, and different Gaussian models

(i.e., Gaussian, lognormal, and generalized Gaussian) should be selected based on the land surface type [62]. Once decomposed, waveform lidar data can be further processed using the same pipeline as discrete lidar data for ecological applications. It should be noted that, although a spatiotemporal analysis approach has been developed to extract features directly from lidar waveforms, it has been mostly used in areas with regular-shaped objects and rarely used in vegetation-related applications [30]. Therefore, this review focuses mainly on discrete or decomposed lidar point clouds hereafter.

Currently, standardized protocols for processing lidar point clouds in ecological studies include four steps: outlier removal, ground point filtering, normalization, and vegetation attribute extraction (Figure 3). Outlier removal aims to remove noisy points caused by high-flying objects or low-level errors, and commonly used algorithms include *k*-means cluster filtering, bilateral filtering, Laplacian operator–based filtering, and mean shift filtering, for example [69], [70]. Ground point filtering aims to identify ground points from lidar data and thereby generate high-precision and high-resolution digital elevation models (DEMs) using interpolation algorithms (e.g., kriging, inverse distance weighting, and triangulated irregular network algorithms) [71], [72]. Many algorithms have been developed to fulfill this task of ground-point filtering by treating terrain as a continuous surface, including slope-based filters, interpolation-based filters, morphology filters, and segmentation-based filters [73], [74]; however, the performance varies significantly under different terrain and vegetation conditions [75], [76]. Special attention needs to be paid to the selection of filtering algorithms based on the characteristics of the study area. Normalization is designed to remove the influence of terrain elevation on lidar height measurements [77]. A normalized point cloud can be calculated by subtracting the terrain elevation from lidar points.

With normalized lidar point clouds, vegetation attributes can be extracted using a variety of approaches. Two well-established types of approach for deriving vegetation attributes are regression-based approaches (also known as area-based approaches) and individual plant segmentation-based approaches [78]. Regression-based approaches estimate vegetation attributes for preestablished grid cells (typically 20–30 m across) by building regression models between field measurements and lidar metrics that summarize the distribution of lidar points within each cell [79], [80]. Among the various regression methods, linear regression has been recognized as one of the most effective because of its ease of interpretation and relatively high accuracy [81]. In addition to linear regression, the random forest method also shows a remarkable performance in deriving vegetation attributes because it can overcome the overfitting problem seen with decision tree algorithms and does not require an assumption of normality of the data [81].

To date, vegetation attributes that have been successfully modeled using regression-based approaches include height, canopy cover, basal area, biomass, and volume at

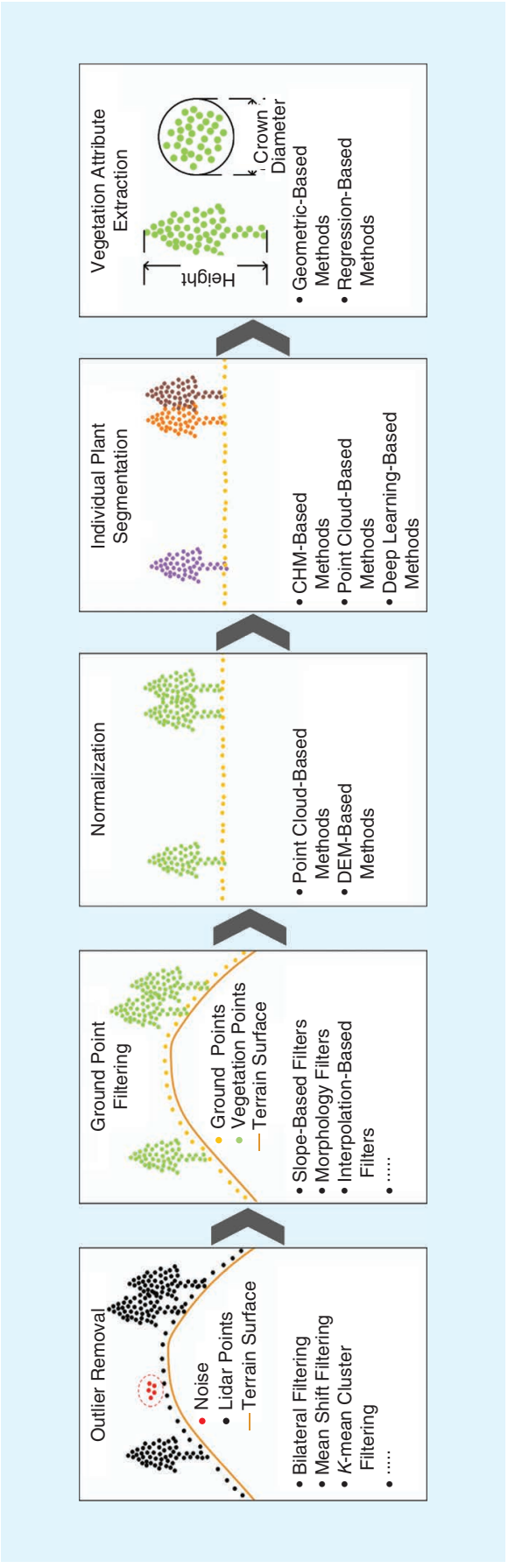

FIGURE 3. The general processing procedure of discrete or decomposed waveform lidar data for ecological studies and example algorithms for each processing step. DEM: digital elevation model.

the community level [37], [82]–[84]. Since regression-based approaches can use a sampling strategy to derive wall-to-wall maps of vegetation attributes [85], they can potentially reduce the need for highly intensive field-based programs and, as a result, offer more spatial details [86].

As the quality of lidar data improves (e.g., point density and accuracy), the demand for deriving vegetation structural attributes at the individual plant level also increases [87]. Individual plant segmentation, i.e., delineating individual plants from the lidar point cloud, has therefore become the prerequisite first step, and the procedures can be generally divided into two categories: canopy height model (CHM)–based methods and point cloud–based methods. CHM-based methods rely on gaps among plants in lidar-derived CHMs and use image segmentation techniques (e.g., watershed segmentation) to delineate the boundary of individual trees [88]–[91]. Point cloud–based methods segment points of each individual plant directly from lidar point clouds [92]–[95]. Vegetation structural attributes at the individual plant level [e.g., tree height, diameter at breast height (DBH), leaf area index (LAI), crown base height, and crown diameter] can then be extracted from individual plant points using geometry-based methods [96]. However, the performance of these algorithms varies significantly across different topographic and vegetation conditions [90], [97]. Depending on the accuracy of tree identification, these methods can be prone to errors in both individual object detection and in tree crown delineation [97], [98] and become less reliable in vegetation stands or communities that are highly vertically complex and have many suppressed and lower-level structures [90].

Recently, deep learning techniques have been successfully used to identify and extract features from 3D lidar point clouds and have segmented individual plants with very high accuracy [99], [100]. This includes separating individual organs (e.g., stem, branches, and leaves) of an individual plant [101], [102] and, therefore, makes quantifying the structural attributes of individual plant organs (e.g., branch length, branching angle, and leaf length) possible [103], [104]. Although deep learning techniques in lidar data processing are still under development, they are expected to play an increasingly important role in the future [105].

THE TRANSITION FROM 2D TO 3D ECOLOGICAL OBSERVATIONS

The highly accurate and informative 3D information provided by lidar sensors is changing the way we study and understand terrestrial ecosystems and is leading the transition from 2D to 3D ecological observations. In this section, we illustrate recent progress in 3D ecological observations and present examples from four terrestrial ecosystems: forest, agricultural, grassland, and urban ecosystems.

FOREST ECOSYSTEMS

Lidar has been widely used to measure forests in 3D at different scales [106]. Among the various lidar platforms, terrestrial laser scanning (TLS) can capture the most accurate and detailed tree structure information and has been largely used to improve the efficiency of forest inventory practices, especially with the help of terrestrial mobile lidar systems (e.g., backpack lidar and mobile lidar) (Figure 4) [19], [43], [107], [108]. Forest structural attributes that can be measured from TLS data include, but are not limited to, DBH, tree height, LAI, clumping index, LAD, leaf inclination angles, crown diameter, crown base height, and crown volume [109]–[114]. Many of the structural attributes derived from lidar data avoid the saturation effect that is typical for passive optical sensors and may even challenge the accuracy of traditional field measurements [115]–[117]. For example, the accuracy of TLS DBH measurements was reported to range from 0.74 to 3.51 cm and tree height measurements from 1.36 to 6.53 m [38], [118], [119]. The accuracy of TLS measurements is primarily influenced by the density and accuracy of point clouds, tree density, and forest type [120], [121]. Moreover, structural features extracted from TLS data also showed the potential to identify tree species by using deep learning techniques [122]–[124]. The combination of TLS volume estimations and tree species information can be used to model aboveground biomass with an accuracy equivalent to that obtained from allometric equations [125, 126]. With the development of stem–leaf separation algorithms, the extraction of tree structure measurements has moved toward quantifying branching architecture, including branching angle, branch diameter, and branch length [25], [127]. Detailed tree structure models from TLS data also provide the opportunity to parameterize 3D radiative transfer models to simulate light distribution and gas exchanges of the canopy [128], [129].

Moving toward the landscape scale, airborne and UAV-borne lidar data are the two main platforms used for measuring wall-to-wall forest attributes [45], [130], [131]. Besides high-resolution topographic products (e.g., digital elevation model and slope) [71], [132], wall-to-wall forest attributes—such as tree height, LAI, LAD, canopy cover, basal area, and aboveground biomass—can also be estimated from lidar data using either object- or area-based approaches (Figure 4) [82], [130], [133]–[138]. Past research has demonstrated strong correlations between field and lidar measurements of height, volume, and biomass, among others (R^2 = 0.43–0.94) [139], with accuracies driven by topographic conditions, lidar point density, scan angle, and forest type [140]. For example, canopy cover calculated from lidar data with large scan angles (>20°) tends to be overestimated [141]. By combining the structure information provided by lidar with optical imagery acquired from satellite or aircraft, vegetation communities in homogeneous forests can be identified more accurately [142], and shrubs can be distinguished from trees more easily than when using optical imagery alone [143].

Airborne and UAV-borne lidar data can also be used to estimate individual tree structural attributes through the

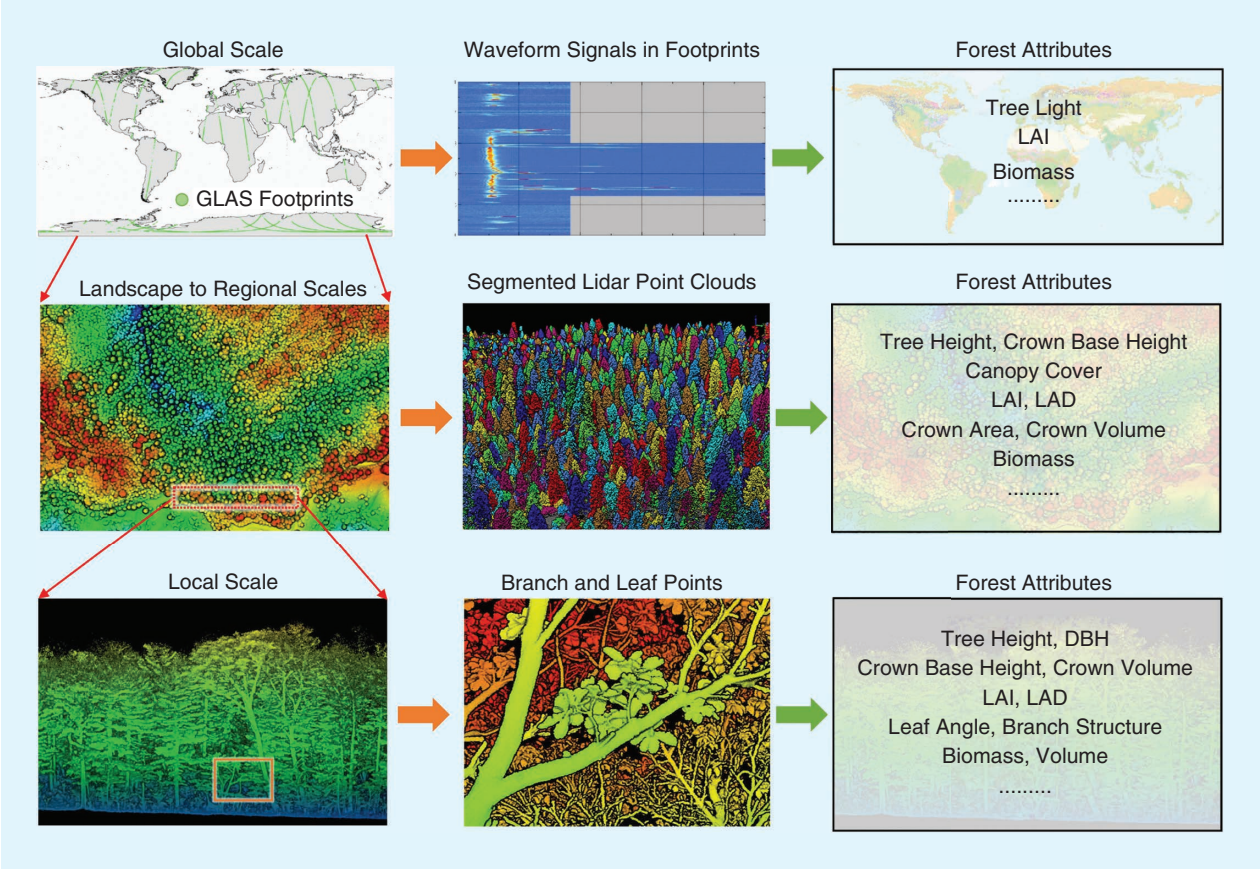

FIGURE 4. Examples of cross-scale forest attribute estimations from lidar observations. At a local scale, detailed and accurate individual tree-level attributes can be obtained from near-surface lidar systems. At landscape to regional scales, forest attributes can be derived either at the individual tree scale or at the group scale. At the global scale, forest attributes are commonly estimated through the fusion of field estimations, near-surface lidar data, spaceborne lidar data (e.g., GLAS full-waveform lidar data), and optical imagery. LAI: leaf area index; LAD: leaf area density; DBH: diameter at breast height.

aid of individual tree segmentation algorithms [92], [93], [144]–[146]. However, the accuracy of individual tree segmentation from airborne and UAV-borne lidar data is not as high as using TLS data [94], [147]–[150]. Attributes that can be extracted are limited to the upper canopy—e.g., tree height, crown base diameter, and crown base height—due to the relatively low point density [140], [151], [152]. UAV-borne lidar data are more preferred for extracting individual tree-level parameters than are airborne lidar data since they have higher point density (>100 points/m^2) [45], [153]. Airborne and UAV-borne acquired lidar data provide unique data sets that can be used to reconstruct and visualize forest landscapes and are increasingly used by forest managers [154], [255].

At regional to global scales, none of the existing lidar platforms can provide complete coverage alone, and the integration of multiplatform lidar data with multisource remote sensing data (e.g., optical imagery or radar data) is the most commonly used method for generating spatially continuous forest products (Figure 4). Field measurements (or TLS measurements) can be first linked with airborne or UAV-borne lidar data to generate landscape-scale estimations, which are then linked with spaceborne lidar data, optical imagery, and radar data to generate regional- and global-scale forest attributes using regression methods [155]–[158]. For example, Su et al. [159], Lefsky [160], and Simard et al. [161] used this strategy to generate tree height maps of the Sierra Nevada of California and of the whole terrestrial biosphere. Hu et al. [162], Nelson et al. [156], and Su et al. [163] also successfully used this strategy to estimate the large-scale distribution of aboveground biomass.

Spaceborne lidar data have played an important role in this strategy since they can alleviate the saturation effect in the upscaling process [162], [163]. GLAS data onboard *ICESat* provided one of the few available spaceborne lidar data sets. Despite the relatively sparse footprints, these data have been used in a number of freely available global forest height and biomass products undertaken with reasonable accuracy (R^2 The newly launched *GEDI* and *ICESat-2* are providing spaceborne data with smaller and denser footprints, which may help improve the accuracy of regional and global forest attributes. However, a combination of both field observations and likely midscale airborne or UAV-borne point clouds is needed to ensure this at continental to global

scales. Regression models built for one specific vegetation type cannot be transferred reliably and accurately to other study sites with different vegetation types [164], [165], and, therefore, collecting airborne or UAV-borne lidar data covering different vegetation types is important for regional to national forest attribute estimation.

Across temporal scales, repeated lidar observations could be used to monitor forest structure dynamics and evaluate large-scale tree competition mechanisms. For example, repeated TLS observations can monitor seasonal forest structure dynamics using the variations in lidar vertical profiles [166], [167]; bitemporal airborne lidar data can be used to detect forest structure changes caused by forest thinning, wildfires, and so on [127], [168]–[171]; and multitemporal lidar data can evaluate tree growth and mortality and investigate tree competition mechanisms [172].

While the application of lidar in the forest ecosystem is more mature compared to its application in other ecosystems, research needs remain. The robustness of forest structural attribute extraction algorithms, for example, still needs improvement. Many algorithms have been derived and applied to specific forest types, topographies, or regions, with less research done on transferability. Although deep learning techniques show great potential in addressing this obstacle, more studies are needed to develop networks with high efficiency and accuracy. Moreover, lidar has been less frequently used in forest ecosystem monitoring due to the lack of temporal lidar data sets, despite the unprecedented 3D observations for forest ecosystems provided. More data collection campaigns to acquire lidar data with a constant time interval (e.g., the National Ecological Observatory Network) are needed.

AGRICULTURAL ECOSYSTEMS

Lidar applications in agricultural systems are still in their early developmental stages. Of areas where lidar data are being applied, the monitoring and modeling of crop growth in agricultural ecosystems show the potential to revolutionize the field of crop phenotyping and function modeling [173], [174].

Current progress in lidar-based crop phenotyping and structure modeling centers mainly on target detection and phenotype extraction [Figure 5(a)]. Target detection aims to detect the location of individual plants or organs. Until recently, most target detection studies have been based on detecting panicles [175], blooms [176], and roots [177], [178] from images. Lidar-based target detection has been recognized as a difficult task due to the challenges in processing the massive, irregular, and unordered lidar data. Jin et al. [99] built a Faster R-CNN deep learning network to detect individual maize plants from terrestrial lidar data, laying the foundation for analyzing crop density and structure variations at the individual plant level [104], [179], [180]. Jin et al. [103] further demonstrated a deep learning–based method for the separation of stem and leaves of an individual maize plant from terrestrial lidar data. Similarly, Malambo et al. [104] detected individual sorghum panicles using a density-based clustering method from terrestrial lidar data. The classification and separation of individual crop organs offer the possibilities to measure crop phenotypes more precisely.

Extracting crop phenotypes from segmented lidar point clouds relies mainly on geometric methods. Compared to traditional manual and image-based methods, lidar-based methods have the advantages of being nondestructive, accurate, and robust [181]–[183]. Currently, TLS and mobile lidar platforms are most commonly used in the extraction of fine phenotypes at the individual plant level [184]–[187], while drone and airborne lidar systems are generally applied to derive large-scale community-level phenotypes [188], [189]. For example, Madec et al. [186], Walter et al. [187], and Jimenez-Berni et al. [190] estimated canopy height and canopy cover of wheat from a mobile lidar system and found them consistent with manual measurements, outperforming imagery-based methods; Jin et al. [103], [165] extracted individual maize height from TLS data with a high agreement with manual measurements ($R^2 > 0.91$) and systematically evaluated the accuracy of phenotypes at stem and leaf levels, including leaf inclination, leaf length, and stem diameter. The high accuracy of phenotype extractions proves that lidar is a promising and valuable tool for the structural modeling of crops and also promotes the development of function modeling in agriculture.

Biomass and yield estimation are indispensable function indicators for crop breeding and agricultural management and are closely linked to crop structure [187], [190]. For example, Walter et al. [187] estimated wheat biomass from lidar projected volume ($r = 0.86$); Jimenez-Berni et al. [190] estimated wheat biomass from a lidar-derived 3D voxel index and a 3D profile index, with an R^2 of 0.93 and 0.92, respectively. Biomass estimation from lidar-derived vegetation indices has been evaluated for various crop types [189]. On the basis of biomass estimation, crop yield can be modeled through a conversion of the harvest index [191]. Moreover, lidar, especially the field lidar phenotyping system, is increasingly used to monitor temporal (e.g., diurnal and seasonal) changes of crop phenotypes (e.g., height, leaf area, and biomass) under environmental stresses, allowing timely observations of phenotype dynamics [Figure 5(b)] [166], [192].

The high price of field phenotyping systems has been one of the major obstacles preventing it from being used at scale. The recent development of near-surface lidar systems (e.g., backpack and unmanned ground vehicle systems) has both reduced the costs and improved the efficiency for collecting lidar data, which may further boost the application of lidar in agricultural systems [193]. However, conventional lidar data lack spectral information, and integrating lidar with other remote sensing sensors (e.g., hyperspectral, thermal, and fluorescence sensors) is indispensable in exploring more diverse structural and function phenotypes [194]–[196].

GRASSLAND ECOSYSTEMS

Grasslands are characterized by very dense but relatively low vegetation. Traditional grassland resource inventories rely heavily on field sampling, which might be inaccurate and time inefficient [197]–[199]. Beyond the spectral information provided by optical remote sensing [200]–[202], we are seeing increasing applications of lidar in grassland ecosystems to extract a range of structural attributes.

Structural attributes are important indicators for characterizing grassland ecosystems [203] and are closely correlated to functional attributes [204]–[206]. However, evaluating structural attributes of grasslands at the individual plant level is difficult even with lidar due to the low height and high density of grass [Figure 6(a)] [199]. At present, structural attributes (e.g., canopy height, canopy volume, and canopy cover) at the community level are the most widely used. Canopy height can be extracted using point- [203], [207], CHM- [199], [208], [209], and voxel-based methods [197], [203], [210]. Point-based methods have been reported to often underestimate grass height for lidar data with relatively low point density [207]. CHM- and voxel-based methods can be highly influenced by the choice of pixel (or voxel) size [197]. Canopy volume can be calculated from lidar data using volume surface differencing approaches [198], voxel counting approaches [204], [210], and convex-hull approaches [210]. Greaves et al. [204] showed that a volume surface differencing approach can generate canopy volume estimations with accuracies similar to those of other approaches but with higher efficiency. Canopy cover is commonly calculated as the ratio of the number of vegetation lidar echoes to the total number of lidar echoes [199].

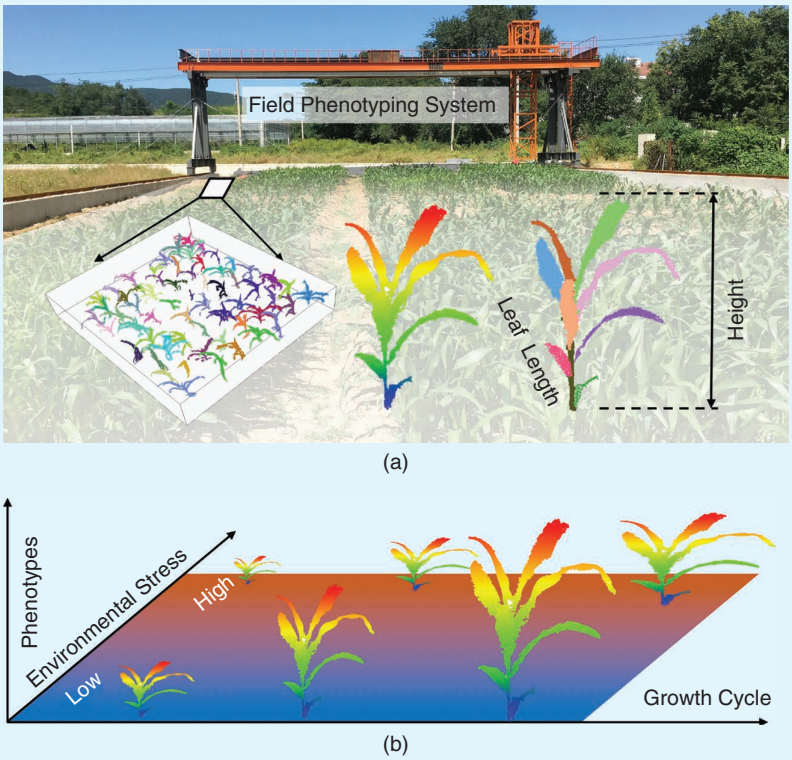

FIGURE 5. Lidar technology enables accurate crop phenotyping and growth monitoring. (a) Individual organ-level crop structural phenotype extraction using a field phenotyping system built by the authors' team ([185]). (b) Crop growth monitoring during the whole growth cycle and environmental stresses.

Using lidar-derived structural attributes as predictors, grassland functional attributes can also be estimated by means of regression-based methods [Figure 6(b)]. Aboveground biomass, a functional indicator of grassland productivity, has been extensively studied by relating destructive field biomass measurements to lidar parameters (e.g., canopy height, canopy volume, and canopy cover) to generate wall-to-wall biomass products [198], [204], [205], [211]. Both Schulze-Brüninghoff et al. [210] and Xu et al. [199] have suggested that lidar-derived canopy height and canopy cover are strongly correlated with aboveground biomass; random forest and stepwise linear regression have been found to produce more robust regression models for aboveground biomass estimation [199]. Moreover, it has been reported that the integration of lidar with spaceborne optical imagery can be used to extrapolate aboveground biomass with a higher accuracy than using only optical imagery [Figure 6(c)] [208].

The applications of lidar in grassland research is still in its infancy as there are still a number of technical questions that need to be addressed. For example, filtering lidar ground points in grasslands, which is the prerequisite step for extracting structural attributes, is a difficult task due to the dense canopy coverage. Structural attributes derived from lidar have been very limited in grassland ecosystems, and more studies are needed to develop ecologically meaningful grassland attributes. Moreover, combining spectral data with structure and functional attributes extracted from lidar data and exploring the relationship between them are another key direction that will need attention in the future [212].

URBAN ECOSYSTEMS

In urban ecosystems, lidar not only allows the quantification of 3D vegetation structures but also can be used to extract and assess buildings. One of the first data sets to be applied in lidar urban applications was airborne lidar data [213], [214]. Recently, terrestrial mobile lidar systems, such as backpack lidar and mobile lidar, have become dominant

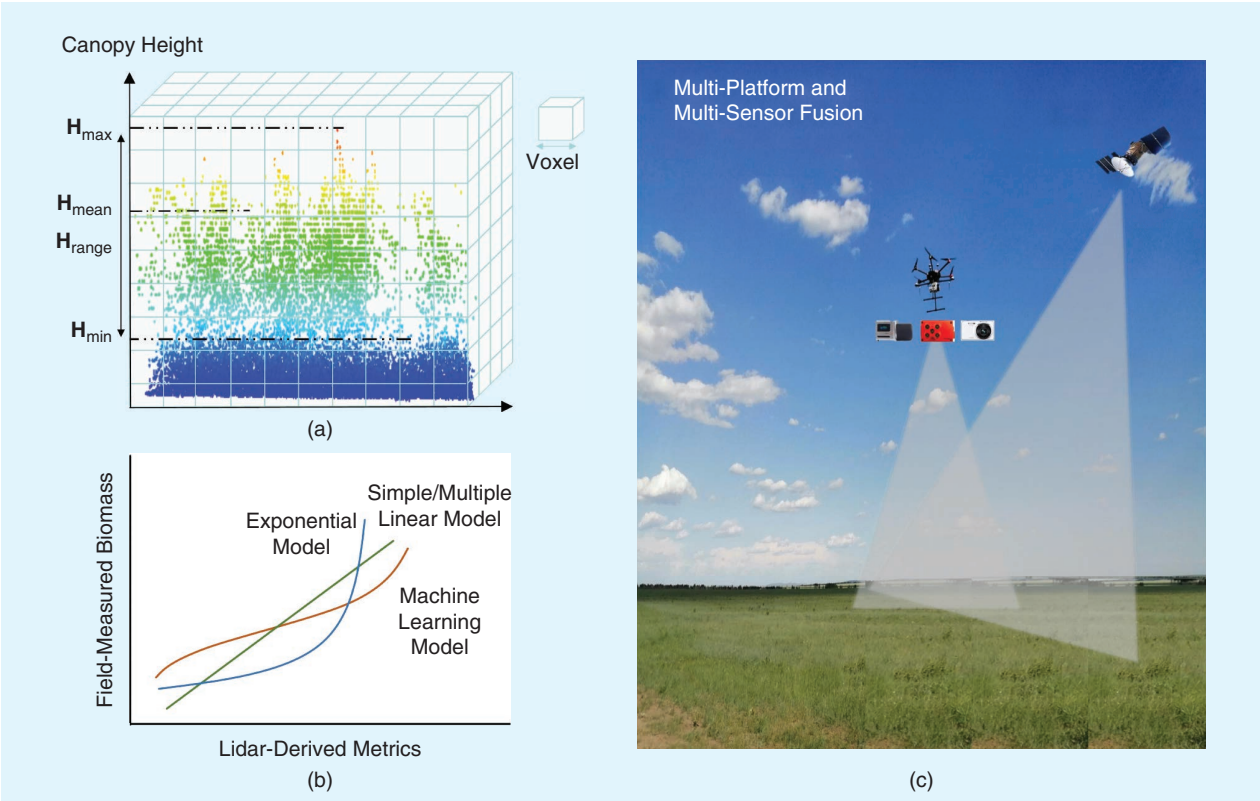

FIGURE 6. Grassland structure and functional attribute estimations using lidar observations. (a) Community-level structural attribute estimation through the voxel-based method; (b) functional attribute (biomass as an example) estimation using the regression-based method; and (c) structure and functional attribute upscaling through the integration of multiplatform and multisensor remote sensing data.

in urban applications due to their unique advantage of allowing data to be collected along roads (Figure 7) [215]. UAV lidar systems have been used less frequently due to the strict flying regulations in urban areas [216].

Unlike in other ecosystems, lidar applications in urban ecosystems have the unique prerequisite of classifying vegetation (e.g., trees and grass cover) and artificial objects (e.g., buildings, power lines, bridges, vehicles, and railways) from lidar point clouds (Figure 7). Various classification algorithms have been introduced that can be generally divided into four categories: pixel-wise classification based on lidar-derived surfaces, object-based segmentation based on lidar-derived surfaces, hierarchical semantic segmentation based on lidar point clouds, and deep learning–based methods.

Pixel-wise classification methods apply traditional machine learning methods (e.g., artificial neural network, maximum likelihood, support vector machine, random forest, Gaussian mixture modeling, rule-based classification, conditional random fields, and Markov random fields) on lidar-derived surfaces (e.g., digital surface models and intensity maps) to classify urban objects [217]–[223]. Object-based segmentation methods, which employ a user-defined procedure to classify segmented objects from lidar-derived surfaces [224]–[226], are designed to avoid the salt-and-pepper effect resulting from pixel-wise classification [227], [228]. Numerous studies have reported that object-based methods can achieve an overall accuracy of >80%, which is higher than what can be derived with pixel-wise methods [229]–[234].

To date, much of the focus in an urban context has been on the identification of large urban objects, while small objects (e.g., trees, street lamps, and power lines) are often neglected. Instead of classifying urban objects from lidar-derived surfaces, hierarchical semantic segmentation methods rely on the entity and contextual information (e.g., points, voxels, planar segments, and objects) within lidar point clouds, which can be used to classify specific urban objects (e.g., roofs, walls, pavements, grass fields, trees, and street lamps) with an accuracy of greater than 90% [235]–[237]. Deep learning–based methods apply convolution neural networks directly to lidar point clouds or lidar-derived surfaces to classify urban objects, and studies have shown that they are highly robust and can achieve an overall accuracy of greater than 96% [238]. Moreover, recent studies have suggested that combining lidar data with color information, such as from aerial or street view photos, can further improve the classification accuracy [218], [224].

Vegetation structure and functional attributes—such as tree height, DBH, crown diameter, crown base height, LAI, tree species, vegetation volume, vegetation coverage, and aboveground biomass—can be extracted from the

classified lidar point clouds in urban environments (Figure 7) [162], [214], [239]–[242]. The accuracy of these extracted attributes is usually higher than in forested areas due to the relatively simple tree species composition and regular tree arrangement in urban ecosystems [239], [243]. One parameter that has drawn the attention of researchers is the urban green space—the public and private urban spaces primarily covered by vegetation [244], [245]. Lidar offers a new way to quantify urban green space from 2D horizontal arrangements to 3D horizontal and vertical arrangements, greatly benefiting studies of urban function connectivity, urban planning and management, and biodiversity [242], [246], [247]. Besides vegetation indices, attributes related to buildings can be also developed from the lidar points, including building height, building mass, building volume, building 3D model type, urban envelope index, and sky openness (Figure 7) [238]], [242], [248]–[252]. These 3D building indices can be used together with urban vegetation attributes to study microclimates and urban flora and fauna, as well as urban planning and management.

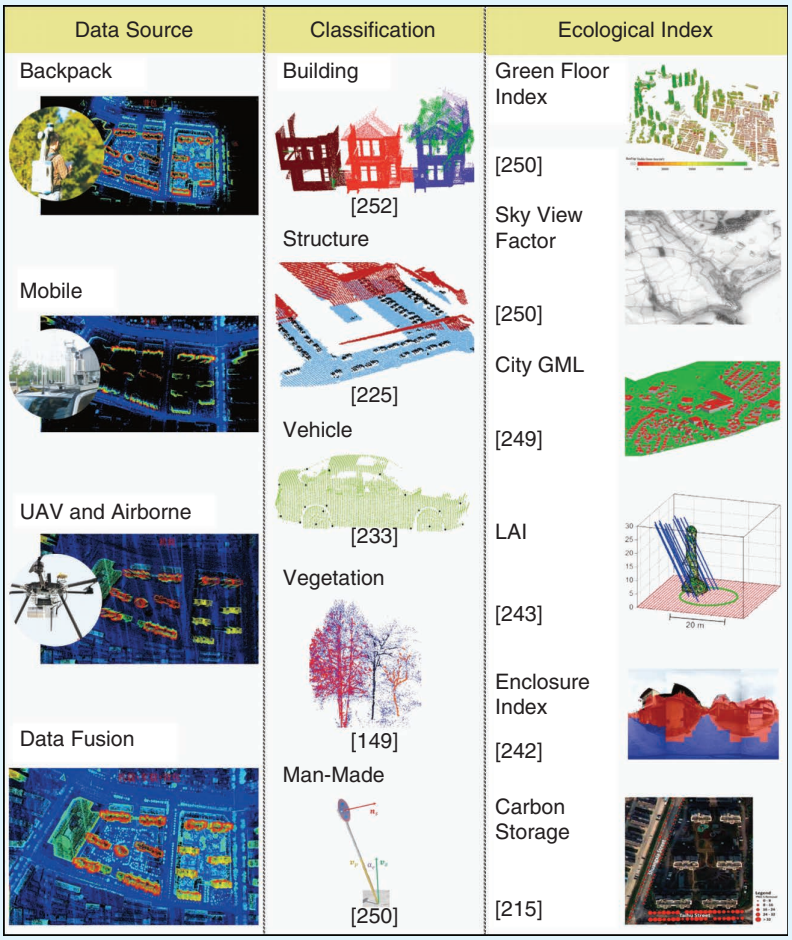

FIGURE 7. 3D lidar observations in urban ecosystems and ecological index examples that can be derived from classified lidar point clouds. Backpack and mobile lidar data can be used to cover areas along and off the road, respectively, while UAV and airborne lidar data can cover a large urban area. The fusion of multiplatform lidar data can provide more complete 3D urban observations. The numbers in brackets represent corresponding references. GML: geography markup language.

Overall, lidar applications in urban ecosystems share common characteristics with other ecosystems in terms of extracting vegetation information, but they involve more efforts in recognizing and processing artificial urban components. The current major obstacles lie in how to handle the huge amount of lidar data at a city scale, especially for data collected by mobile lidar systems. Moreover, how to incorporate lidar-derived 3D parameters into urban ecological studies and modeling still needs to be further explored.

LIDAR OBSERVATIONS TO INFORM 3D ECOLOGICAL MODELING

The observation and quantification of ecological attributes from lidar data are providing key insights into ecological modeling studies. In forest ecosystems, accurate forest structure observations from lidar allow the integration of vegetation structure information into solar radiation modeling, vegetation dynamic modeling, and biodiversity modeling across scales, which ultimately can lead to a better understanding of forest ecosystems. Approaches like voxel-based transfer models and discrete anisotropic radiative transfer models can be used to simulate accurate 3D radiation distribution [128], [253], [254] and thereby investigate the influence of canopy structure on the canopy light regime and photosynthetic partitioning [129]. Accurate 3D tree structural attributes also provide the opportunity to validate hypotheses in current vegetation dynamic models. For example, Su et al. [256] used TLS data to prove that canopy architecture displays a strong spatial variability along climate gradients and to reject the current hypothesis in vegetation dynamic models of a constant ratio between canopy height and canopy size. Tao et al. [257] found that canopy height exhibits a hump-shaped correlation with water availability, rejecting the prevailing assumption that canopy height follows a linear correlation with water availability. Xue et al. [258] further proved that tuning vegetation dynamic models with lidar-derived attributes can lead

to significantly different carbon modeling results. These studies suggest that interpreting the spatial and temporal dynamics of forest structure and incorporating them into the current dynamic vegetation models are necessary and important research directions [256].

Moreover, the vertical dimension provided by lidar data enables much more comprehensive and accurate descriptions of animal habitats [259]. Forest canopy structure is a very important factor influencing animal behavior (e.g., nesting, hunting, and breeding) that is often neglected in current niche modeling studies [26], [260]. Feeding niche models with lidar-derived vegetation structural attributes has the potential to overcome this obstacle. For example, Zhao et al. [261] showed that lidar-derived structural attributes could better characterize fisher (a rare mammal) dens; García-Feced et al. [262] and North et al. [263] found that using lidar-derived snag trees and the cover of tall trees could predict California spotted owl nesting habitats; Loarie et al. [264] used lidar-derived vegetation structure to explain the hunting behavior of male lions; and Blakey et al. [265] and Eichhorn et al. [266] used lidar-derived structure information to understand how deer, birds, and bats choose their habitats. Coops et al. [267] proposed a 3D index using lidar data capturing the three main components of vertical and horizontal vegetation structure (i.e., height, cover, and complexity) and proved that this index can be used to predict avian species richness more accurately than using climate or land cover data alone. However, animals of different taxonomic groups interact with forest canopy differently. Thus, investigating the influence of 3D forest canopy structure on a wider range of animals can benefit our understanding of the correlation between canopy structure and biodiversity.

In agricultural ecosystems, lidar has improved the accuracy of crop growth modeling. Crop growth models aim to simulate the crop growth cycle with the input of environmental variables (e.g., temperature, precipitation, soil moisture, and fertilizer) [268], [269]. Lidar can provide detailed and accurate structural traits at an individual organ level, which could be a robust information source for validating and calibrating crop growth models. Additionally, the 3D light regime of agricultural ecosystems can be more accurately modeled with the aid of 3D radiative transfer models [270], which can refine the environmental input of crop growth models. The combination of improved crop growth models and accurate lidar observations could ultimately lead to more efficient crop management. However, the incorporation of lidar data into crop growth models is still in its very early stages. A recent study by Liu et al. [271] used a function–structure–plant model to provide *in silico* experiments for exploring the feasibility of lidar-based phenotype estimation (e.g., a green area index) with machine learning methods. More studies are still urgently needed to investigate the potential of lidar in the crop growth modeling process.

In grassland ecosystems, airborne and UAV lidar data have been used to model spatial heterogeneity and biodiversity [211], [272]. For example, Jansen et al. [273] used lidar-derived structural attributes to model the influence of grazing on the spatial heterogeneity of a bunchgrass prairie ecosystem; Moeslund et al. [274] successfully used airborne lidar data to assess the local biodiversity of grasslands and meadows in bushes; and Marcinkowska-Ochtyra et al. [275] and Fisher et al. [276] modeled the distribution of grassland invasive species. These results, combined with biomass modeling results from lidar [199], can ultimately provide much more accurate information for managing and protecting grassland ecosystems. However, currently, studies in this direction are still few in number. More studies are urgently needed to link lidar-derived structural attributes with functional attributes to better simulate grassland ecosystem processes.

In urban ecosystems, detailed 3D information of built and vegetation structures can be assimilated into models to understand urban microclimates, investigate urban biodiversity, and ensure the health of urban ecosystems. The 3D arrangements of buildings and vegetation can alter the spatial and temporal variability of solar radiation [277]–[281], and assimilating the 3D information of buildings and vegetation into climate models can improve the accuracy of microclimate simulations [282]–[285]. Moreover, urban ecosystems have become an important habitat for both flora and fauna, and anthropogenic activities are important factors influencing the biodiversity of urban ecosystems. The integration of lidar-derived information into biodiversity studies can help better describe the spatial distribution of vegetation and animal species in an urban environment [286], [287]. Modeled vegetation and animal distribution can be further used to analyze and predict human health risks (e.g., exposure to pollen and mosquito abundance) [288]–[290]. In addition, lidar data can be used to model risks related to power lines, flooding, and so on, and thus help in devising management plans that ensure the health of urban ecosystems [196], [291]–[295].

To conclude, lidar-derived 3D information is an important input for ecological models. The integration of lidar observations into ecological models can improve our understanding and may even challenge our existing theories on ecological processes. Despite the consensus on the importance of integrating lidar observations into ecological models, this process is still in the early stages across ecosystems. Incorporating 3D lidar observations across scales and ecosystems need to be extensively explored in future studies.

FROM 3D TO THE MULTIDIMENSIONAL BIG DATA ERA

In conjunction with optical remote sensing and field surveys, lidar has played a crucial role in the development of 3D ecological observations and modeling. Lidar data have allowed researchers to gain new insights and gather finer details about ecological processes [256], [257]. Nevertheless, increasing demands have emerged to expand our ecological observations from 3D (i.e., X, Y, and Z) to multiple

dimensions (i.e., X, Y, Z and the spectral and temporal dimensions) to compensate for the weaknesses of single-type or single-date remote sensing data.

MOVING TOWARD THE FUSION OF STRUCTURAL AND SPECTRAL INFORMATION

Lidar has the known limitation of lacking spectral information. The intensity recorded by lidar sensors is highly influenced by signal attenuation and multipath effects [142], [296]. Although there have been significant efforts in developing algorithms to calibrate lidar intensity [52], [297]–[301], it is still difficult to generate physically meaningful spectral reflectance values or cross-platform comparable intensity values [296]. Moreover, most current lidar systems have only one band in the near-infrared wavelength range. Recent developments in dual-band and multiband lidar sensors show the potential to address the limitations of single-band lidar systems [57], [302]–[304], yet the costs of dual-band and multiband lidar sensors are high and their capability to derive cross-platform comparable reflectance values is still questionable [305]. Another solution for addressing this problem is to fuse lidar data with multispectral and hyperspectral data to compensate for the weakness of each type of data (i.e., lidar data lack spectral information and multispectral and hyperspectral data lack structural information). Studies have proven that by fusing lidar data with multispectral or hyperspectral data, the resulting data can outperform the single type of data in terms of species classification, vegetation mapping, biomass estimation, and so on [163], [224], [305]–[308]. Therefore, the simultaneous collection of multisource remote sensing data remains the trend for future ecological observations.

MOVING TOWARD REGULAR TIME-SERIES ECOLOGICAL OBSERVATIONS

Current available lidar data sets have been used to create valuable benchmarks of ecosystem attributes (e.g., vegetation attributes, snow depth, and tree line information) [163], [309]–[311], which can then be used as important baselines to evaluate ecosystem dynamics under the background of global climate change. However, we need to monitor vegetation dynamics using multitemporal data so that we can further understand ecological processes and predict possible ecosystems changes in future climate scenarios. Thus far, such studies have been dominated by the use of time-series optical images and radar data across the globe (e.g., *Landsat TM*, MODIS, *Sentinel-1*, and *Sentinel-2*) [5], [312]–[314]. Although there are studies using multitemporal lidar data to investigate ecosystem dynamics [169], [170], [172], [192], [315], collecting time-series lidar data with a constant time interval has been sporadic due to the paucity of spaceborne lidar sensors and the high cost of collecting airborne and terrestrial lidar data. Recent developments in near-surface lidar platforms (e.g., backpack lidar and UAV lidar) have greatly reduced the cost and increased the flexibility of lidar data collection. Moreover, newly launched spaceborne lidar sensors (e.g., *GEDI* and *ICESat-2*) can provide global-scale time-series lidar observations. This progress in lidar sensors has made the collection of time-series lidar data possible.

MOVING TOWARD THE ERA OF BIG DATA

It has been estimated that the data streaming from the National Aeronautics and Space Administration active space missions alone represent more than 1.7 gigabytes [316]. With the accumulation of multisource, multitemporal, and multiscale remote sensing data, the amount of ecological observations will grow explosively [317]. Remote sensing–based ecological observations are stepping into the big data era.

Upon the transition of ecological observations from 3D to the multidimensional big data era, three common challenges are being faced across ecosystems. First, how should lidar data be fused with multispectral and hyperspectral data? The majority of existing studies have simply compressed the 3D lidar data into 2D vegetation attributes and then fused the derived vegetation attributes with those from multispectral and hyperspectral data directly based on spatial information [307], [318]. Further studies are needed to explore the possibility of fusing lidar data with multispectral and hyperspectral data in 3D so that the potential of multisource data can be fully explored. The use of 3D radiative transfer models in the data fusion process might be a potential solution to this question.

Second, how should changes from multitemporal lidar data sets be detected? Due to the changes in lidar sensors, viewing angles, vegetation conditions, and so on, lidar data collected at different times and from different platforms can hardly be directly compared [319]. The registration error of multitemporal lidar data may further increase the difficulty of detecting ecosystem changes [41]. Finding a method that can be used to compare lidar data across platforms and time is urgently needed.

Third, how should the accumulation of big remote sensing data be handled? With the increasing amount of data acquisition, the computation pressure of data processing is becoming a new challenge. New opportunities for data exploration may exist by using deep learning techniques with computation acceleration techniques (e.g., parallel processing and graphic processing unit acceleration). In addition, new data sharing policies and platforms are also urgently needed to promote widespread data availability.

CONCLUSIONS

Lidar has become an indispensable tool for ecological observations and modeling and will play an increasingly important role in the future. The development of lidar sensors, especially emerging near-surface lidar systems, significantly improves the flexibility and reduces the cost of lidar data acquisition. Robust and efficient lidar data processing algorithms are evolving, fostering the development of 3D ecological observations. Many studies have been conducted to extract accurate 3D ecosystem attributes from lidar data

across scales (from individual organs to global scales) and ecosystems (from forest to agricultural to grassland to urban ecosystems). These 3D attributes offer new sources of data for modeling ecosystem processes.

Although new insights and refined details have been achieved through the integration of lidar observations into ecological models, new efforts for developing and improving current ecological models should still be a high research priority. With the accumulation of a wide range of remote sensing data, ecological observations are moving from 3D to an era of multidimensional big data. How to handle and fully explore the potential of time-series multiplatform data through data fusion is becoming a new challenge for the research community, but it also opens new opportunities for understanding ecological processes.

ACKNOWLEDGMENTS

This work was supported in part by the Strategic Priority Research Program of the Chinese Academy of Sciences (CAS) (XDA19050401 and XDA24020202), the National Key R&D Program of China (2017YFC0503905), the Frontier Science Key Programs of the CAS (QYZDY-SSW-SMC011), the National Natural Science Foundation of China (41871332,31971575,41901358), the CAS President's International Fellowship Initiative (2019VTA0007), and a Natural Sciences and Engineering Research Council of Canada Discovery grant (RGPIN-2018-03851).

AUTHOR INFORMATION

Qinghua Guo (guo.qinghua@gmail.com) is with the Institute of Ecology, College of Urban and Environmental Science, Peking University, Beijing, China. Yanjun Su and Qinghua Guo contributed equally to this work.

Yanjun Su (ysu@ibcas.ac.cn) is with the State Key Laboratory of Vegetation and Environmental Change, Institute of Botany, Chinese Academy of Sciences, Beijing, China, and also with the University of Chinese Academy of Sciences. Yanjun Su and Qinghua Guo contributed equally to this work.

Tianyu Hu (tianyuhu@ibcas.ac.cn) is with the State Key Laboratory of Vegetation and Environmental Change, Institute of Botany, Chinese Academy of Sciences, Beijing, China, and also with the University of Chinese Academy of Sciences.

Hongcan Guan (guanhongcan@gmail.com) is with the State Key Laboratory of Vegetation and Environmental Change, Institute of Botany, Chinese Academy of Sciences, Beijing, China, and also with the University of Chinese Academy of Sciences.

Shichao Jin (jinshichao1993@gmail.com) is with the State Key Laboratory of Vegetation and Environmental Change, Institute of Botany, Chinese Academy of Sciences, Beijing, China, and also with the University of Chinese Academy of Sciences.

Jing Zhang (eve.zhangj@gmail.com) is with the State Key Laboratory of Vegetation and Environmental Change, Institute of Botany, Chinese Academy of Sciences, Beijing, China, and also with the University of Chinese Academy of Sciences.

Xiaoxia Zhao (xxia_zhao@163.com) is with the State Key Laboratory of Vegetation and Environmental Change, Institute of Botany, Chinese Academy of Sciences, Beijing, China, and also with the University of Chinese Academy of Sciences.

Kexin Xu (kexin_xu4ever@163.com) is with the State Key Laboratory of Vegetation and Environmental Change, Institute of Botany, Chinese Academy of Sciences, Beijing, China, and also with the University of Chinese Academy of Sciences.

Dengjie Wei (weidengjie@ibcas.ac.cn) is with the State Key Laboratory of Vegetation and Environmental Change, Institute of Botany, Chinese Academy of Sciences, Beijing, China, and also with the University of Chinese Academy of Sciences.

Maggi Kelly (maggi@berkeley.edu) is with the Department of Environmental Science, Policy, and Management, University of California Berkeley, Berkeley, California, USA, and also with the Division of Agriculture and Natural Resources, University of California Davis.

Nicholas C. Coops (nicholas.coops@ubc.ca) is with the Department of Forest Resource Management, University of British Columbia, Vancouver, British Columbia, Canada.

REFERENCES

[1] R. Wang and J. A. Gamon, "Remote sensing of terrestrial plant biodiversity," *Remote Sens. Environ.*, vol. 231, p. 111,218, Sept. 2019. doi: 10.1016/j.rse.2019.111218.

[2] M. A. Wulder et al., "Current status of Landsat program, science, and applications," *Remote Sens. Environ.*, vol. 225, pp. 127–147, May 2019. doi: 10.1016/j.rse.2019.02.015.

[3] P. Aplin, "Remote sensing: Ecology," *Prog. Phys. Geogr.*, vol. 29, no. 1, pp. 104–113, 2005. doi: 10.1191/030913305pp437pr.

[4] J. T. Kerr and M. Ostrovsky, "From space to species: Ecological applications for remote sensing," *Trends Ecol. Evol.*, vol. 18, no. 6, pp. 299–305, 2003. doi: 10.1016/S0169-5347(03)00071-5.

[5] R. E. Kennedy et al., "Bringing an ecological view of change to Landsat-based remote sensing," *Front. Ecol. Environ.*, vol. 12, no. 6, pp. 339–346, 2014. doi: 10.1890/130066.

[6] D. P. Roy, Y. Jin, P. Lewis, and C. O. Justice, "Prototyping a global algorithm for systematic fire-affected area mapping using MODIS time series data," *Remote Sens. Environ.*, vol. 97, no. 2, pp. 137–162, 2005. doi: 10.1016/j.rse.2005.04.007.

[7] D. P. Roy et al., "Landsat-8: Science and product vision for terrestrial global change research," *Remote Sens. Environ.*, vol. 145, pp. 154–172, Apr. 2014. doi: 10.1016/j.rse.2014.02.001.

[8] T. Hermosilla, M. A. Wulder, J. C. White, N. C. Coops, G. W. Hobart, and L. B. Campbell, "Mass data processing of time series Landsat imagery: Pixels to data products for forest monitoring," *Int. J. Digit. Earth*, vol. 9, no. 11, pp. 1035–1054, 2016. doi: 10.1080/17538947.2016.1187673.

[9] G. P. Asner, B. Braswell, D. S. Schimel, and C. A. Wessman, "Ecological research needs from multiangle remote sensing

data," *Remote Sens. Environ.*, vol. 63, no. 2, pp. 155–165, 1998. doi: 10.1016/S0034-4257(97)00139-9.

[10] S. Liang and A. Strahler, "Retrieval of surface BRDF from multiangle remotely sensed data," *Remote Sens. Environ.*, vol. 50, no. 1, pp. 18–30, 1994. doi: 10.1016/0034-4257(94)90091-4.

[11] A. S. Olpenda, K. Stereńczak, and K. Będkowski, "Modeling solar radiation in the forest using remote sensing data: A review of approaches and opportunities," *Remote Sens.*, vol. 10, no. 5, p. 694, 2018. doi: 10.3390/rs10050694.

[12] J. Chen, X. Li, T. Nilson, and A. Strahler, "Recent advances in geometrical optical modelling and its applications," *Remote Sens. Rev.*, vol. 18, nos. 2–4, pp. 227–262, 2000. doi: 10.1080/02757250009532391.

[13] J. L. Widlowski et al., "The fourth phase of the radiative transfer model intercomparison (RAMI) exercise: Actual canopy scenarios and conformity testing," *Remote Sens. Environ.*, vol. 169, pp. 418–437, Nov. 2015. doi: 10.1016/j.rse.2015.08.016.

[14] M. Huesca, M. García, K. L. Roth, A. Casas, and S. L. Ustin, "Canopy structural attributes derived from AVIRIS imaging spectroscopy data in a mixed broadleaf/conifer forest," *Remote Sens. Environ.*, vol. 182, pp. 208–226, Sept. 2016. doi: 10.1016/j.rse.2016.04.020.

[15] M. C. Hansen et al., "Mapping tree height distributions in Sub-Saharan Africa using Landsat 7 and 8 data," *Remote Sens. Environ.*, vol. 185, pp. 221–232, Nov. 2016. doi: 10.1016/j.rse.2016.02.023.

[16] Q. Ma, Y. Su, L. Luo, L. Li, M. Kelly, and Q. Guo, "Evaluating the uncertainty of Landsat-derived vegetation indices in quantifying forest fuel treatments using bi-temporal LiDAR data," *Ecol. Indic.*, vol. 95, pp. 298–310, Dec. 2018. doi: 10.1016/j.ecolind.2018.07.050.

[17] C. Qian et al., "An integrated GNSS/INS/LiDAR-SLAM positioning method for highly accurate forest stem mapping," *Remote Sens.*, vol. 9, no. 1, p. 3, 2017. doi: 10.3390/rs9010003.

[18] S. E. Reutebuch, H.-E. Andersen, and R. J. McGaughey, "Light detection and ranging (LIDAR): An emerging tool for multiple resource inventory," *J. For.*, vol. 103, no. 6, pp. 286–292, 2005.

[19] J. Shao et al., "SLAM-aided forest plot mapping combining terrestrial and mobile laser scanning," *ISPRS J. Photogramm. Remote Sens.*, vol. 163, pp. 214–230, May 2020. doi: 10.1016/j.isprsjprs.2020.03.008.

[20] J. L. Lovell, D. L. B. Jupp, G. J. Newnham, N. C. Coops, and D. S. Culvenor, "Simulation study for finding optimal lidar acquisition parameters for forest height retrieval," *Forest Ecol. Manage.*, vol. 214, nos. 1–3, pp. 398–412, doi: 10.1016/j.foreco.2004.07.077.

[21] S. Hancock et al., "Characterising forest gap fraction with terrestrial lidar and photography: An examination of relative limitations," *Agric. Forest Meteorol.*, vols. 189–190, pp. 105–114, June 2014. doi: 10.1016/j.agrformet.2014.01.012.

[22] A. S. Whitehurst, A. Swatantran, J. B. Blair, R. Dubayah, and M. A. Hofton, "Characterization of canopy layering in forested ecosystems using full waveform lidar," *Remote Sens.*, vol. 5, no. 4, pp. 2014–2036, 2013. doi: 10.3390/rs5042014.

[23] F. Zhao et al., "Measuring gap fraction, element clumping index and LAI in Sierra Forest stands using a full-waveform ground-based lidar," *Remote Sens. Environ.*, vol. 125, pp. 73–79, Oct. 2012. doi: 10.1016/j.rse.2012.07.007.

[24] F. Hosoi and K. Omasa, "Factors contributing to accuracy in the estimation of the woody canopy leaf area density profile using 3D portable lidar imaging," *J. Exp. Bot.*, vol. 58, no. 12, pp. 3463–3473, 2007. doi: 10.1093/jxb/erm203.

[25] Y. Li et al., "Retrieval of tree branch architecture attributes from terrestrial laser scan data using a Laplacian algorithm," *Agric. Forest Meteorol.*, vol. 284, p. 107,874, Apr. 2020. doi: 10.1016/j.agrformet.2019.107874.

[26] A. B. Davies and G. P. Asner, "Advances in animal ecology from 3D-LiDAR ecosystem mapping," *Trends Ecol. Evol.*, vol. 29, no. 12, pp. 681–691, 2014. doi: 10.1016/j.tree.2014.10.005.

[27] K. T. Vierling, L. A. Vierling, W. A. Gould, S. Martinuzzi, and R. Clawges, "Lidar: Shedding new light on habitat characterization and modeling," *Front. Ecol. Environ.*, vol. 6, no. 2, pp. 90–98, 2008. doi: 10.1890/070001.

[28] J. Q. Chambers et al., "Regional ecosystem structure and function: Ecological insights from remote sensing of tropical forests," *Trends Ecol. Evol.*, vol. 22, no. 8, pp. 414–423, Aug. 2007. doi: 10.1016/j.tree.2007.05.001.

[29] R. Nelson, W. Krabill, and G. MacLean, "Determining forest canopy characteristics using airborne laser data," *Remote Sens. Environ.*, vol. 15, no. 3, pp. 201–212, 1984. doi: 10.1016/0034-4257(84)90031-2.

[30] C. Mallet and F. Bretar, "Full-waveform topographic lidar: State-of-the-art," *ISPRS J. Photogramm. Remote Sens.*, vol. 64, no. 1, pp. 1–16, 2009. doi: 10.1016/j.isprsjprs.2008.09.007.

[31] R. D. Ketchum, "Airborne laser profiling of the Arctic pack ice," *Remote Sens. Environ.*, vol. 2, pp. 41–52, 1971–1973. doi: 10.1016/0034-4257(71)90076-9.

[32] H. Arp, J. C. Criesbach, and J. P. Burns, "Mapping in tropical forests—a new approach using the laser APR," *Photogramm. Eng. Remote Sens.*, vol. 48, no. 1, pp. 91–100, 1982.

[33] R. Nelson, "How did we get here? An early history of forestry lidar1," *Can. J. Remote Sens.*, vol. 39, no. sup1, pp. S6–S17, June 2013. doi: 10.5589/m13-011.

[34] J. Bufton et al., "Airborne lidar for profiling of surface topography," *Opt. Eng.*, vol. 30, no. 1, pp. 72–79, 1991. doi: 10.1117/12.55770.

[35] G. T. Raber, J. R. Jensen, S. R. Schill, and K. Schuckman, "Creation of digital terrain models using an adaptive lidar vegetation point removal process," *Photogramm. Eng. Remote Sens.*, vol. 68, no. 12, pp. 1307–1315, 2002.

[36] S. E. Reutebuch, R. J. McGaughey, H.-E. Andersen, and W. W. Carson, "Accuracy of a high-resolution lidar terrain model under a conifer forest canopy," *Can. J. Remote Sens.*, vol. 29, no. 5, pp. 527–535, 2003. doi: 10.5589/m03-022.

[37] M. A. Lefsky, W. B. Cohen, G. G. Parker, and D. J. Harding, "Lidar Remote Sensing for Ecosystem Studies: Lidar, an emerging remote sensing technology that directly measures the three-dimensional distribution of plant canopies, can accurately estimate vegetation structural attributes and should be of particular interest to forest, landscape, and global ecologists," *BioScience*, vol. 52, no. 1, pp. 19–30, 2002. doi: 10.1641/0006-3568(2002)052[0019:LRSFES]2.0.CO;2.

[38] H. G. Maas, A. Bienert, S. Scheller, and E. Keane, "Automatic forest inventory parameter determination from terrestrial laser

scanner data," *Int. J. Remote Sens.*, vol. 29, no. 5, pp. 1579–1593, 2008. doi: 10.1080/01431160701736406.

[39] L. Fan, W. Powrie, J. Smethurst, and P. M. Atkinson, "The effect of short ground vegetation on terrestrial laser scans at a local scale," *ISPRS J. Photogramm. Remote Sens.*, vol. 95, pp. 42–52, Sept. 2014. doi: 10.1016/j.isprsjprs.2014.06.003.

[40] T. Hilker et al., "A simple technique for co-registration of terrestrial LiDAR observations for forestry applications," *Remote Sens. Lett.*, vol. 3, no. 3, pp. 239–247, 2012. doi: 10.1080/01431161.2011.565815.

[41] H. Guan et al., "A novel framework to automatically fuse multiplatform LiDAR data in forest environments based on tree locations," *IEEE Trans. Geosci. Remote Sens.*, vol. 58, no. 3, pp. 2165–2177, Mar. 2020. doi: 10.1109/TGRS.2019.2953654.

[42] H. Guan et al., "A marker-free method for registering multiscan terrestrial laser scanning data in forest environments," *ISPRS J. Photogramm. Remote Sens.*, vol. 166, pp. 82–94, Aug. 2020. doi: 10.1016/j.isprsjprs.2020.06.002.

[43] X. Liang et al., "In-situ measurements from mobile platforms: An emerging approach to address the old challenges associated with forest inventories," *ISPRS J. Photogramm. Remote Sens.*, vol. 143, pp. 97–107, Sept. 2018. doi: 10.1016/j.isprsjprs.2018.04.019.

[44] M. Pierzchała, P. Giguère, and R. Astrup, "Mapping forests using an unmanned ground vehicle with 3D LiDAR and graph-SLAM," *Comput. Electron. Agric.*, vol. 145, pp. 217–225, Feb. 2018. doi: 10.1016/j.compag.2017.12.034.

[45] Q. Guo et al., "An integrated UAV-borne lidar system for 3D habitat mapping in three forest ecosystems across China," *Int. J. Remote Sens.*, vol. 38, nos. 8–10, pp. 2954–2972, 2017. doi: 10.1080/01431161.2017.1285083.

[46] H. Tang, R. Dubayah, M. Brolly, S. Ganguly, and G. Zhang, "Large-scale retrieval of leaf area index and vertical foliage profile from the spaceborne waveform lidar (GLAS/ICESat)," *Remote Sens. Environ.*, vol. 154, pp. 8–18, Nov. 2014. doi: 10.1016/j.rse.2014.08.007.

[47] W. Qi, S. Saarela, J. Armston, G. Ståhl, and R. Dubayah, "Forest biomass estimation over three distinct forest types using TanDEM-X InSAR data and simulated GEDI lidar data," *Remote Sens. Environ.*, vol. 232, p. 111,283, 2019. doi: 10.1016/j.rse.2019.111283.

[48] J. J. Degnan, "Scanning, multibeam, single photon lidars for rapid, large scale, high resolution, topographic and bathymetric mapping," *Remote Sens.*, vol. 8, no. 11, p. 958, 2016. doi: 10.3390/rs8110958.

[49] A. M. Pawlikowska, A. Halimi, R. A. Lamb, and G. S. Buller, "Single-photon three-dimensional imaging at up to 10 kilometers range," *Opt. Express*, vol. 25, no. 10, pp. 11,919–11,931, 2017. doi: 10.1364/OE.25.011919.

[50] B. Smith et al., "Land ice height-retrieval algorithm for NASA's ICESat-2 photon-counting laser altimeter," *Remote Sens. Environ.*, vol. 233, p. 111,352, Nov. 2019. doi: 10.1016/j.rse.2019.111352.

[51] A. M. Wallace et al., "Design and evaluation of multispectral LiDAR for the recovery of arboreal parameters," *IEEE Trans. Geosci. Remote Sens.*, vol. 52, no. 8, pp. 4942–4954, 2014. doi: 10.1109/TGRS.2013.2285942.

[52] S. Shi, S. Song, W. Gong, L. Du, B. Zhu, and X. Huang, "Improving backscatter intensity calibration for multispectral LiDAR," *IEEE Geosci. Remote Sens. Lett.*, vol. 12, no. 7, pp. 1421–1425, 2015. doi: 10.1109/LGRS.2015.2405573.

[53] S. Kaasalainen, T. Lindroos, and J. Hyyppa, "Toward hyperspectral Lidar: Measurement of spectral backscatter intensity with a supercontinuum laser source," *IEEE Geosci. Remote Sens. Lett.*, vol. 4, no. 2, pp. 211–215, 2007. doi: 10.1109/LGRS.2006.888848.

[54] Y. Chen et al., "A 10-nm spectral resolution hyperspectral LiDAR system based on an acousto-optic tunable filter," *Sensors*, vol. 19, no. 7, p. 1620, 2019. doi: 10.3390/s19071620.

[55] L. Du et al., "Estimation of rice leaf nitrogen contents based on hyperspectral LIDAR," *Int. J. Appl. Earth Observ. Geoinf.*, vol. 44, pp. 136–143, Feb. 2016. doi: 10.1016/j.jag.2015.08.008.

[56] J. Sun et al., "Estimating leaf chlorophyll status using hyperspectral lidar measurements by PROSPECT model inversion," *Remote Sens. Environ.*, vol. 212, pp. 1–7, June 2018. doi: 10.1016/j.rse.2018.04.024.

[57] M. Kukkonen et al., "Comparison of multispectral airborne laser scanning and stereo matching of aerial images as a single sensor solution to forest inventories by tree species," *Remote Sens. Environ.*, vol. 231, p. 111,208, Sept. 2019. doi: 10.1016/j.rse.2019.05.027.

[58] J. R. Roussel et al., "lidR: An R package for analysis of airborne laser scanning (ALS) data," *Remote Sens. Environ.*, vol. 251, no. 12, p. 112,061, 2020. doi: 10.1016/j.rse.2020.112061.

[59] U. Stilla, W. Yao, and B. Jutzi, "Detection of weak laser pulses by full waveform stacking," *Int. Arch. Photogramm. Remote Sens. Spatial Inform. Sci.*, vol. 36, no. Part 3, pp. W49A, 2007. 2007.

[60] C. Mallet, F. Bretar, M. Roux, U. Soergel, and C. Hepke, "Relevance assessment of full-waveform lidar data for urban area classification," *ISPRS J. Photogramm. Remote Sens.*, vol. 66, no. 6, pp. S71–S84, 2011. doi: 10.1016/j.isprsjprs.2011.09.008.

[61] J. Reitberger, P. Krzystek, and U. Stilla, "Analysis of full waveform LIDAR data for the classification of deciduous and coniferous trees," *Int. J. Remote Sens.*, vol. 29, no. 5, pp. 1407–1431, 2008. doi: 10.1080/01431160701736448.

[62] A. Chauve et al., "Processing full-waveform LiDar data in an alpine coniferous forest: Assessing terrain and tree height quality," *Int. J. Remote Sens.*, vol. 30, no. 19, p. 27, 2009. doi: 10.1080/01431160903023009.

[63] W. Wagner, A. Ullrich, V. Ducic, T. Melzer, and N. Studnicka, "Gaussian decomposition and calibration of a novel small-footprint full-waveform digitising airborne laser scanner," *ISPRS J. Photogramm. Remote Sens.*, vol. 60, no. 2, pp. 100–112, 2006. doi: 10.1016/j.isprsjprs.2005.12.001.

[64] Y. Qin, T. T. Vu, and Y. Ban, "Toward an optimal algorithm for LiDAR waveform decomposition," *IEEE Geosci. Remote Sens. Lett.*, vol. 9, no. 3, pp. 482–486, May 2012. doi: 10.1109/LGRS.2011.2172676.

[65] M. A. Hofton, J.-B. Minster, and J. B. Blair, "Decomposition of laser altimeter waveforms," *IEEE Trans. Geosci. Remote Sens.*, vol. 38, no. 4, pp. 1989–1996, 2000. doi: 10.1109/36.851780.

[66] B. Jutzi and U. Stilla, "Range determination with waveform recording laser systems using a Wiener Filter," *ISPRS J. Pho-*

togramm. Remote Sens., vol. 61, no. 2, pp. 95–107, 2006. doi: 10.1016/j.isprsjprs.2006.09.001.

[67] A. Persson, U. Soedarman, J. Toepel, and S. Ahlberg, "Visualization and analysis of full-waveform airborne laser scanner data," *Int. Arch. Photogramm. Remote Sens. Spatial Inf. Sci.*, vol. 36, no. 3, p. W19, 2005.

[68] S. Hernandez-Marin, A. M. Wallace, and G. J. Gibson, "Bayesian analysis of lidar signals with multiple returns," *IEEE Trans. Pattern Anal. Mach. Intell.*, vol. 29, no. 12, pp. 2170–2180, 2007. doi: 10.1109/TPAMI.2007.1122.

[69] X.-F. Han, J. S. Jin, M.-J. Wang, W. Jiang, L. Gao, and L. Xiao, "A review of algorithms for filtering the 3D point cloud," *Signal Process. Image Commun.*, vol. 57, pp. 103–112, Sept. 2017. doi: 10.1016/j.image.2017.05.009.

[70] H. Chen et al., "A fast voxel-based method for outlier removal in laser measurement," *Int. J. Precis. Eng. Manuf.*, vol. 20, no. 6, pp. 915–925, 2019. doi: 10.1007/s12541-019-00113-0.

[71] Q. Guo, W. Li, H. Yu, and O. Alvarez, "Effects of topographic variability and lidar sampling density on several DEM interpolation methods," *Photogramm. Eng. Remote Sens.*, vol. 76, no. 6, pp. 701–712, 2010. doi: 10.14358/PERS.76.6.701.

[72] C. Chen, Y. Li, N. Zhao, and C. Yan, "Robust interpolation of DEMs from Lidar-derived elevation data," *IEEE Trans. Geosci. Remote Sens.*, vol. 56, no. 2, pp. 1059–1068, 2018. doi: 10.1109/TGRS.2017.2758795.

[73] D. Mongus and B. Žalik, "Parameter-free ground filtering of LiDAR data for automatic DTM generation," *ISPRS J. Photogramm. Remote Sens.*, vol. 67, pp. 1–12, Jan. 2012. doi: 10.1016/j.isprsjprs.2011.10.002.

[74] X. Zhao, Q. Guo, Y. Su, and B. Xue, "Improved progressive TIN densification filtering algorithm for airborne LiDAR data in forested areas," *ISPRS J. Photogramm. Remote Sens.*, vol. 117, pp. 79–91, July 2016. doi: 10.1016/j.isprsjprs.2016.03.016.

[75] A. L. Montealegre, M. T. Lamelas, and J. de la Riva, "A comparison of open-source LiDAR filtering algorithms in a Mediterranean forest environment," *IEEE J. Sel. Topics Appl. Earth Observ. Remote Sens.*, vol. 8, no. 8, pp. 4072–4085, 2015. doi: 10.1109/JSTARS.2015.2436974.

[76] X. Zhao, Y. Su, W. Li, T. Hu, J. Liu, and Q. Guo, "A comparison of LiDAR filtering algorithms in vegetated mountain areas," *Canadian J. Remote Sens.*, vol. 44, no. 4, pp. 287–298, 2018. doi: 10.1080/07038992.2018.1481738.

[77] A. Khosravipour, A. K. Skidmore, T. Wang, M. Isenburg, and K. Khoshelham, "Effect of slope on treetop detection using a LiDAR Canopy Height Model," *ISPRS J. Photogramm. Remote Sens.*, vol. 104, pp. 44–52, June 2015. doi: 10.1016/j.isprsjprs.2015.02.013.

[78] J. C. White, N. C. Coops, M. A. Wulder, M. Vastaranta, T. Hilker, and P. Tompalski, "Remote sensing technologies for enhancing forest inventories: A review," *Can. J. Remote Sens.*, vol. 42, no. 5, pp. 619–641, 2016. doi: 10.1080/07038992.2016.1207484.

[79] E. Næsset, "Predicting forest stand characteristics with airborne scanning laser using a practical two-stage procedure and field data," *Remote Sens. Environ.*, vol. 80, no. 1, pp. 88–99, 2002. doi: 10.1016/S0034-4257(01)00290-5.

[80] J. C. White, M. A. Wulder, A. Varhola, and M. Vastaranta, "A best practices guide for generating forest inventory attributes from airborne laser scanning data using an area-based approach," *For. Chro.*, vol. 89, no. 6, pp. 722–723, 2013. doi: 10.5558/tfc2013-132.

[81] U. Grömping, "Variable importance assessment in regression: Linear regression versus random forest," *Am. Stat.*, vol. 63, no. 4, pp. 308–319, 2009. doi: 10.1198/tast.2009.08199.

[82] H.-E. Andersen, R. J. McGaughey, and S. E. Reutebuch, "Estimating forest canopy fuel parameters using LIDAR data," *Remote Sens. Environ.*, vol. 94, no. 4, pp. 441–449, 2005. doi: 10.1016/j.rse.2004.10.013.

[83] M. A. Lefsky, D. Harding, W. Cohen, G. Parker, and H. H. Shugart, "Surface lidar remote sensing of basal area and biomass in deciduous forests of eastern Maryland, USA," *Remote Sens. Environ.*, vol. 67, no. 1, pp. 83–98, 1999. doi: 10.1016/S0034-4257(98)00071-6.

[84] E. Næsset and T. Økland, "Estimating tree height and tree crown properties using airborne scanning laser in a boreal nature reserve," *Remote Sens. Environ.*, vol. 79, no. 1, pp. 105–115, 2002. doi: 10.1016/S0034-4257(01)00243-7.

[85] C. W. Bater, M. A. Wulder, N. C. Coops, R. F. Nelson, T. Hilker, and E. Nasset, "Stability of sample-based scanning-LiDAR-derived vegetation metrics for forest monitoring," *IEEE Trans. Geosci. Remote Sens.*, vol. 49, no. 6, pp. 2385–2392, 2011. doi: 10.1109/TGRS.2010.2099232.

[86] J. C. White, M. A. Wulder, T. Hermosilla, N. C. Coops, and G. W. Hobart, "A nationwide annual characterization of 25 years of forest disturbance and recovery for Canada using Landsat time series," *Remote Sens. Environ.*, vol. 194, pp. 303–321, June 2017. doi: 10.1016/j.rse.2017.03.035.

[87] C. Véga and S. Durrieu, "Multi-level filtering segmentation to measure individual tree parameters based on Lidar data: Application to a mountainous forest with heterogeneous stands," *Int. J. Appl. Earth Observ. Geoinf.*, vol. 13, no. 4, pp. 646–656, 2011. doi: 10.1016/j.jag.2011.04.002.

[88] D.-A. Kwak, W.-K. Lee, J.-H. Lee, G. S. Biging, and P. Gong, "Detection of individual trees and estimation of tree height using LiDAR data," *J. For. Res.*, vol. 12, no. 6, pp. 425–434, 2007. doi: 10.1007/s10310-007-0041-9.

[89] A. Khosravipour, A. K. Skidmore, M. Isenburg, Y. Hussin, and T. Wang, "Generating pit-free canopy height models from airborne lidar," *Photogramm. Eng. Remote Sens.*, vol. 80, no. 9, pp. 863–872, 2014. doi: 10.14358/PERS.80.9.863.

[90] Q. Yang et al., "The influence of vegetation characteristics on individual tree segmentation methods with airborne LiDAR data," *Remote Sens.*, vol. 11, no. 23, p. 2880, 2019. doi: 10.3390/rs11232880.

[91] J. Yang, Z. Kang, S. Cheng, Z. Yang, and P. H. Akwensi, "An individual tree segmentation method based on watershed algorithm and 3D spatial distribution analysis from airborne LiDAR point clouds," *IEEE J. Sel. Topics Appl. Earth Observ. Remote Sens.*, vol. 13, pp. 1055–1057, 2020. doi: 10.1109/JSTARS.2020.2979369.

[92] W. Li, Q. Guo, M. K. Jakubowski, and M. Kelly, "A new method for segmenting individual trees from the lidar point cloud,"

Photogramm. Eng. Remote Sens., vol. 78, no. 1, pp. 75–84, 2012. doi: 10.14358/PERS.78.1.75.

[93] X. Lu, Q. Guo, W. Li, and J. Flanagan, "A bottom-up approach to segment individual deciduous trees using leaf-off lidar point cloud data," *ISPRS J. Photogramm. Remote Sens.*, vol. 94, pp. 1–12, Aug. 2014. doi: 10.1016/j.isprsjprs.2014.03.014.

[94] S. Tao, F. Wu, Q. Guo, et al. "Segmenting tree crowns from terrestrial and mobile LiDAR data by exploring ecological theories," *ISPRS J. Photogramm. Remote Sens.*, vol. 110, pp. 66–76, Dec. 2015. doi: 10.1016/j.isprsjprs.2015.10.007.

[95] W. Yao, P. Krzystek, and M. Heurich, "Tree species classification and estimation of stem volume and DBH based on single tree extraction by exploiting airborne full-waveform LiDAR data," *Remote Sens. Environ.*, vol. 123, pp. 368–380, Aug. 2012. doi: 10.1016/j.rse.2012.03.027.

[96] Á. Casas, M. García, R. B. Siegel, A. Koltunov, C. Ramírez, and S. Ustin, "Burned forest characterization at single-tree level with airborne laser scanning for assessing wildlife habitat," *Remote Sens. Environ.*, vol. 175, pp. 231–241, Mar. 2016. doi: 10.1016/j.rse.2015.12.044.

[97] M. K. Jakubowski, W. Li, Q. Guo, and M. Kelly, "Delineating individual trees from LiDAR data: A comparison of vector-and raster-based segmentation approaches," *Remote Sens.*, vol. 5, no. 9, pp. 4163–4186, 2013. doi: 10.3390/rs5094163.

[98] J. Hyyppa, "Detecting and estimating attributes for single trees using laser scanner," *Photogramm. J. Finland*, vol. 16, pp. 27–42, Jan. 1999.

[99] S. Jin et al., "Deep learning: Individual maize segmentation from terrestrial lidar data using faster R-CNN and regional growth algorithms," *Front. Plant Sci.*, vol. 9, p. 866, June 2018. doi: 10.3389/fpls.2018.00866.

[100] H. Hamraz, N. B. Jacobs, M. A. Contreras, and C. Clark, "Deep learning for conifer/deciduous classification of airborne LiDAR 3D point clouds representing individual trees," *ISPRS J. Photogramm. Remote Sens.*, vol. 158, pp. 219–230, Dec. 2019. doi: 10.1016/j.isprsjprs.2019.10.011.

[101] S. Jin et al., "Separating the structural components of maize for field phenotyping using terrestrial LiDAR data and deep convolutional neural networks," *IEEE Trans. Geosci. Remote Sens.*, vol. 58, no. 4, pp. 2644–2658, 2020. doi: 10.1109/TGRS.2019.2953092.

[102] W. Shi, R. van de Zedde, H. Jiang, and G. Kootstra, "Plant-part segmentation using deep learning and multi-view vision," *Biosyst. Eng.*, vol. 187, pp. 81–95, Nov. 2019. doi: 10.1016/j.biosystemseng.2019.08.014.

[103] S. Ji et al., "Stem–leaf segmentation and phenotypic trait extraction of individual maize using terrestrial LiDAR data," *IEEE Trans. Geosci. Remote Sens.*, vol. 57, no. 3, pp. 1336–1346, 2018. doi: 10.1109/TGRS.2018.2866056.

[104] L. Malambo, S. C. Popescu, D. W. Horne, N. A. Pugh, and W. L. Rooney, "Automated detection and measurement of individual sorghum panicles using density-based clustering of terrestrial lidar data," *ISPRS J. Photogramm. Remote Sens.*, vol. 149, pp. 1–13, Mar. 2019. doi: 10.1016/j.isprsjprs.2018.12.015.

[105] L. Ma, Y. Liu, X. Zhang, Y. Xe, G. Yin, and B. A. Johnson, "Deep learning in remote sensing applications: A meta-analysis and review," *ISPRS J. Photogramm. Remote Sens.*, vol. 152, pp. 166–177, June 2019. doi: 10.1016/j.isprsjprs.2019.04.015.

[106] M. Kelly and S. D. Tommaso, "Mapping forests with Lidar provides flexible, accurate data with many uses," *Calif. Agric.*, vol. 69, no. 1, pp. 14–20, 2015. doi: 10.3733/ca.v069n01p14.

[107] E. Hyyppä et al., "Accurate derivation of stem curve and volume using backpack mobile laser scanning," *ISPRS J. Photogramm. Remote Sens.*, vol. 161, pp. 246–262, Mar. 2020. doi: 10.1016/j.isprsjprs.2020.01.018.

[108] A. E. L. Stovall, K. J. Anderson-Teixeira, and H. H. Shugart, "Assessing terrestrial laser scanning for developing non-destructive biomass allometry," *Forest Ecol. Manage.*, vol. 427, pp. 217–229, Nov. 2018. doi: 10.1016/j.foreco.2018.06.004.

[109] M. Koreň, M. Mokroš, and T. Bucha, "Accuracy of tree diameter estimation from terrestrial laser scanning by circle-fitting methods," *Int. J. Appl. Earth Observ. Geoinf.*, vol. 63, pp. 122–128, Dec. 2017. doi: 10.1016/j.jag.2017.07.015.

[110] Y. Li, Q. Guo, Y. Su, S. Tao, K. Zhao, and G. Xua, "Retrieving the gap fraction, element clumping index, and leaf area index of individual trees using single-scan data from a terrestrial laser scanner," *ISPRS J. Photogramm. Remote Sens.*, vol. 130, pp. 308–316, Aug. 2017. doi: 10.1016/j.isprsjprs.2017.06.006.

[111] W. Lin, Y. Meng, Z. Qiu, S. Zhang, and J. Wu, "Measurement and calculation of crown projection area and crown volume of individual trees based on 3D laser-scanned point-cloud data," *Int. J. Remote Sens.*, vol. 38, no. 4, pp. 1083–1100, 2017. doi: 10.1080/01431161.2016.1265690.

[112] N. Saarinen et al., "Feasibility of terrestrial laser scanning for collecting stem volume information from single trees," *ISPRS J. Photogramm. Remote Sens.*, vol. 123, pp. 140–158, Jan. 2017. doi: 10.1016/j.isprsjprs.2016.11.012.

[113] G. Zheng and L. M. Moskal, "Leaf orientation retrieval from terrestrial laser scanning (TLS) data," *IEEE Trans. Geosci. Remote Sens.*, vol. 50, no. 10, pp. 3970–3979, 2012. doi: 10.1109/TGRS.2012.2188533.

[114] X. Zhu et al., "Improving leaf area index (LAI) estimation by correcting for clumping and woody effects using terrestrial laser scanning," *Agric. For. Meteorol.*, vol. 263, pp. 276–286, Dec. 2018. doi: 10.1016/j.agrformet.2018.08.026.

[115] X. Liang et al., "International benchmarking of terrestrial laser scanning approaches for forest inventories," *ISPRS J. Photogramm. Remote Sens.*, vol. 144, pp. 137–179, Oct. 2018. doi: 10.1016/j.isprsjprs.2018.06.021.

[116] X. Liang et al., "Forest in situ observations using unmanned aerial vehicle as an alternative of terrestrial measurements," *For. Ecosyst.*, vol. 6, no. 1, p. 20, 2019. doi: 10.1186/s40663-019-0173-3.

[117] Y. Wang et al., "Is field-measured tree height as reliable as believed – A comparison study of tree height estimates from field measurement, airborne laser scanning and terrestrial laser scanning in a boreal forest," *ISPRS J. Photogramm. Remote Sens.*, vol. 147, pp. 132–145, Jan. 2019. doi: 10.1016/j.isprsjprs.2018.11.008.

[118] V. Kankare et al., "Outlook for the single-tree-level forest inventory in Nordic countries," in *The Rise of Big Spatial Data (Lecture Notes in Geoinformation and Cartography)*, I. Ivan, A. Singleton, J.

Horák, and T. Inspektor, Eds. Berlin: Springer-Verlag, 2017, pp. 183–195.

[119] X. Liang and J. Hyyppä, "Automatic stem mapping by merging several terrestrial laser scans at the feature and decision levels," *Sensors*, vol. 13, no. 2, pp. 1614–1634, 2013. doi: 10.3390/s130201614.

[120] V. Kankare, E. Puttonen, M. Holopainen, and J. Hyyppä, "The effect of TLS point cloud sampling on tree detection and diameter measurement accuracy," *Remote Sens. Lett.*, vol. 7, no. 5, pp. 495–502, 2016. doi: 10.1080/2150704X.2016.1157639.

[121] P. Pueschel, G. Newnham, G. Rock, T. Udelhoven, W. Werner, and J. Hill, "The influence of scan mode and circle fitting on tree stem detection, stem diameter and volume extraction from terrestrial laser scans," *ISPRS J. Photogramm. Remote Sens.*, vol. 77, pp. 44–56, Mar. 2013. doi: 10.1016/j.isprsjprs.2012.12.001.

[122] M. Åkerblom, P. Raumonen, R. Mäkipää, and M. Kaasalainen, "Automatic tree species recognition with quantitative structure models," *Remote Sens. Environ.*, vol. 191, pp. 1–12, Mar. 2017. doi: 10.1016/j.rse.2016.12.002.

[123] A. Hovi, L. Korhonen, J. Vauhkonen, and I. Korpela, "LiDAR waveform features for tree species classification and their sensitivity to tree- and acquisition related parameters," *Remote Sens. Environ.*, vol. 173, pp. 224–237, Feb. 2016. doi: 10.1016/j.rse.2015.08.019.

[124] Y. Shi, T. Wang, A. K. Skidmore, and M. Heurich, "Important LiDAR metrics for discriminating forest tree species in Central Europe," *ISPRS J. Photogramm. Remote Sens.*, vol. 137, pp. 163–174, Mar. 2018. doi: 10.1016/j.isprsjprs.2018.02.002.

[125] J. Gonzalez de Tanago et al., "Estimation of above-ground biomass of large tropical trees with terrestrial LiDAR," *Methods Ecol. Evol.*, vol. 9, no. 2, pp. 223–234, 2018. doi: 10.1111/2041-210X.12904.

[126] A. E. L. Stovall, A. G. Vorster, R. S. Anderson, P. H. Evangelista, and H. H. Shugart, "Non-destructive aboveground biomass estimation of coniferous trees using terrestrial LiDAR," *Remote Sens. Environ.*, vol. 200, pp. 31–42, Oct. 2017. doi: 10.1016/j.rse.2017.08.013.

[127] M. Bremer, V. Wichmann, and M. Rutzinger, "Multi-temporal fine-scale modelling of Larix decidua forest plots using terrestrial LiDAR and hemispherical photographs," *Remote Sens. Environ.*, vol. 206, pp. 189–204, Mar. 2018. doi: 10.1016/j.rse.2017.12.023.

[128] W. Li, Q. Guo, S. Tao, and Y. Su, "VBRT: A novel voxel-based radiative transfer model for heterogeneous three-dimensional forest scenes," *Remote Sens. Environ.*, vol. 206, pp. 318–335, Mar. 2018. doi: 10.1016/j.rse.2017.12.043.

[129] T. S. Magney et al., "LiDAR canopy radiation model reveals patterns of photosynthetic partitioning in an Arctic shrub," *Agric. For. Meteorol.*, vol. 221, pp. 78–93, May 2016. doi: 10.1016/j.agrformet.2016.02.007.

[130] M. Bouvier, S. Durrieu, R. A. Fournier, et al. "Generalizing predictive models of forest inventory attributes using an area-based approach with airborne LiDAR data," *Remote Sens. Environ.*, vol. 156, pp. 322–334, Jan. 2015. doi: 10.1016/j.rse.2014.10.004.

[131] M. A. Wulder et al., "Lidar sampling for large-area forest characterization: A review," *Remote Sens. Environ.*, vol. 121, pp. 196–209, June 2012. doi: 10.1016/j.rse.2012.02.001.

[132] F. Pirotti, A. Guarnieri, and A. Vettore, "State of the art of ground and aerial laser scanning technologies for high-resolution topography of the Earth surface," *Euro. J. Remote Sens.*, vol. 46, no. 1, pp. 66–78, Jan. 2013. doi: 10.5721/EuJRS20134605.

[133] M. L. Clark, D. B. Clark, and D. A. Roberts, "Small-footprint lidar estimation of sub-canopy elevation and tree height in a tropical rain forest landscape," *Remote Sens. Environ.*, vol. 91, no. 1, pp. 68–89, 2004. doi: 10.1016/j.rse.2004.02.008.

[134] L. Korhonen, I. Korpela, J. Heiskanen, and M. Maltamo, "Airborne discrete-return LIDAR data in the estimation of vertical canopy cover, angular canopy closure and leaf area index," *Remote Sens. Environ.*, vol. 115, no. 4, pp. 1065–1080, 2011. doi: 10.1016/j.rse.2010.12.011.

[135] E. Lindberg, K. Olofsson, J. Holmgren, and H. Olsson, "Estimation of 3D vegetation structure from waveform and discrete return airborne laser scanning data," *Remote Sens. Environ.*, vol. 118, pp. 151–161, Mar. 2012. doi: 10.1016/j.rse.2011.11.015.

[136] S. C. Popescu and K. Zhao, "A voxel-based lidar method for estimating crown base height for deciduous and pine trees," *Remote Sens. Environ.*, vol. 112, no. 3, pp. 767–781, 2008. doi: 10.1016/j.rse.2007.06.011.

[137] S. Tao et al., "Airborne lidar-derived volume metrics for aboveground biomass estimation: A comparative assessment for conifer stands," *Agric. For. Meteorol.*, vols. 198–199, pp. 24–32, Nov.–Dec. 2014. doi: 10.1016/j.agrformet.2014.07.008.

[138] X. Zhu, J. Liu, A. K. Skidmore, J. Premier, and M. Heurich, "A voxel matching method for effective leaf area index estimation in temperate deciduous forests from leaf-on and leaf-off airborne LiDAR data," *Remote Sens. Environ.*, vol. 240, p. 111,696, Apr. 2020. doi: 10.1016/j.rse.2020.111696.

[139] M. J. Sumnall, R. A. Hill, and S. A. Hinsley, "Comparison of small-footprint discrete return and full waveform airborne lidar data for estimating multiple forest variables," *Remote Sens. Environ.*, vol. 173, pp. 214–223, Feb. 2016. doi: 10.1016/j.rse.2015.07.027.

[140] M. K. Jakubowski, Q. Guo, and M. Kelly, "Tradeoffs between lidar pulse density and forest measurement accuracy," *Remote Sens. Environ.*, vol. 130, pp. 245–253, Mar. 2013. doi: 10.1016/j.rse.2012.11.024.

[141] Q. Ma, Y. Su, and Q. Guo, "Comparison of canopy cover estimations from airborne LiDAR, aerial imagery, and satellite imagery," *IEEE J. Sel. Topics Appl. Earth Observ. Remote Sens.*, vol. 10, no. 9, pp. 4225–4236, 2017. doi: 10.1109/JSTARS.2017.2711482.

[142] Y. Su et al., "A vegetation mapping strategy for conifer forests by combining airborne LiDAR data and aerial imagery," *Can. J. Remote Sens.*, vol. 42, no. 1, pp. 1–15, 2016. doi: 10.1080/07038992.2016.1131114.

[143] I. Zahidi, B. Yusuf, A. Hamedianfar, H. Z. M. Shafri, and T. A. Mohamed, "Object-based classification of QuickBird image and low point density LIDAR for tropical trees and shrubs mapping," *Euro. J. Remote Sens.*, vol. 48, no. 1, pp. 423–446, 2015. doi: 10.5721/EuJRS20154824.

[144] Q. Chen, D. Baldocchi, P. Gong, and M. Kelly, "Isolating individual trees in a savanna woodland using small footprint lidar data," *Photogramm. Eng. Remote Sens.*, vol. 72, no. 8, pp. 923–932, 2006. doi: 10.14358/PERS.72.8.923.

[145] L. I. Duncanson, B. D. Cook, G. C. Hurtt, and R. O. Dubayah, "An efficient, multi-layered crown delineation algorithm for mapping individual tree structure across multiple ecosystems," *Remote Sens. Environ.*, vol. 154, pp. 378–386, Nov. 2014. doi: 10.1016/j.rse.2013.07.044.

[146] C. Paris, D. Valduga, and L. Bruzzone, "A hierarchical approach to three-dimensional segmentation of LiDAR data at single-tree level in a multilayered forest," *IEEE Trans. Geosci. Remote Sens.*, vol. 54, no. 7, pp. 4190–4203, 2016. doi: 10.1109/TGRS.2016.2538203.

[147] A. Burt, M. Disney, and K. Calders, "Extracting individual trees from lidar point clouds using treeseg," *Methods Ecol. Evol.*, vol. 10, no. 3, pp. 438–445, 2019. doi: 10.1111/2041-210X.13121.

[148] L. Li, D. Li, H. Zhu, and Y. Li, "A dual growing method for the automatic extraction of individual trees from mobile laser scanning data," *ISPRS J. Photogramm. Remote Sens.*, vol. 120, pp. 37–52, Oct. 2016. doi: 10.1016/j.isprsjprs.2016.07.009.

[149] S. Xu, N. Ye, S. Xu, and F. Zhu, "A supervoxel approach to the segmentation of individual trees from LiDAR point clouds," *Remote Sens. Lett.*, vol. 9, no. 6, pp. 515–523, 2018. doi: 10.1080/2150704X.2018.1444286.

[150] L. Zhong, L. Cheng, H. Xu, Y. Wu, Y. Chen, and M. Li, "Segmentation of individual trees from TLS and MLS data," *IEEE J. Sel. Topics Appl. Earth Observ. Remote Sens.*, vol. 10, no. 2, pp. 774–787, 2017. doi: 10.1109/JSTARS.2016.2565519.

[151] A. Kato, L. M. Moskal, P. Schiess, M. E. Swanson, D. Calhoun, and W. Stuetzle, "Capturing tree crown formation through implicit surface reconstruction using airborne lidar data," *Remote Sens. Environ.*, vol. 113, no. 6, pp. 1148–1162, 2009. doi: 10.1016/j.rse.2009.02.010.

[152] L. Luo, Q. Zhai, Y. Su, Q. Guo, L. Luo, Q. Zhai, and Q. Ma, "Simple method for direct crown base height estimation of individual conifer trees using airborne LiDAR data," *Opt. Express*, vol. 26, no. 10, pp. A562–A578, 2018. doi: 10.1364/OE.26.00A562.

[153] T. R. Goodbody, N. C. Coops, P. L. Marshall, P. Tompalski, and P. Crawford, "Unmanned aerial systems for precision forest inventory purposes: A review and case study," *For. Chro.*, vol. 93, no. 1, pp. 71–81, 2017. doi: 10.5558/tfc2017-012.

[154] F. Morsdorf, E. Meier, B. Kötz, K. I. Itten, M. Dobbertin, and B. Allgöwer, "LIDAR-based geometric reconstruction of boreal type forest stands at single tree level for forest and wildland fire management," *Remote Sens. Environ.*, vol. 92, no. 3, pp. 353–362, 2004. doi: 10.1016/j.rse.2004.05.013.

[155] L. Li, Q. Guo, S. Tao, M. Kelly, and G. Xu, "Lidar with multi-temporal MODIS provide a means to upscale predictions of forest biomass," *ISPRS J. Photogramm. Remote Sens.*, vol. 102, pp. 198–208, Apr. 2015. doi: 10.1016/j.isprsjprs.2015.02.007.

[156] R. Nelson et al., "Lidar-based estimates of aboveground biomass in the continental US and Mexico using ground, airborne, and satellite observations," *Remote Sens. Environ.*, vol. 188, pp. 127–140, 2017. doi: 10.1016/j.rse.2016.10.038.

[157] N. C. Coops, T. R. H. Goodbody, and L. Cao, "Four steps to extend drone use in research," *Nature*, vol. 572, no. 7770, pp. 433–435, 2019. doi: 10.1038/d41586-019-02474-y.

[158] G. Matasci et al., "Large-area mapping of Canadian boreal forest cover, height, biomass and other structural attributes using Landsat composites and lidar plots," *Remote Sens. Environ.*, vol. 209, pp. 90–106, May 2018. doi: 10.1016/j.rse.2017.12.020.

[159] Y. Su, Q. Ma, and Q. Guo, "Fine-resolution forest tree height estimation across the Sierra Nevada through the integration of spaceborne LiDAR, airborne LiDAR, and optical imagery," *Int. J. Digit. Earth*, vol. 10, no. 3, pp. 307–323, 2017. doi: 10.1080/17538947.2016.1227380.

[160] M. A. Lefsky, "A global forest canopy height map from the Moderate Resolution Imaging Spectroradiometer and the Geoscience Laser Altimeter System," *Geophys. Res. Lett.*, vol. 37, no. 15, p. L15401, 2010. doi: 10.1029/2010GL043622.

[161] M. Simard, N. Pinto, J. B. Fisher, and A. Baccini, "Mapping forest canopy height globally with spaceborne lidar," *J. Geophys. Res., Biogeosci.*, vol. 116, no. G4, p. G04021, 2011. doi: 10.1029/2011JG001708.

[162] T. Hu et al., "Mapping global forest aboveground biomass with spaceborne LiDAR, optical imagery, and forest inventory data," *Remote Sens.*, vol. 8, no. 7, p. 565, 2016. doi: 10.3390/rs8070565.

[163] Y. Su et al., "Spatial distribution of forest aboveground biomass in China: Estimation through combination of spaceborne lidar, optical imagery, and forest inventory data," *Remote Sens. Environ.*, vol. 173, pp. 187–199, Feb. 2016. doi: 10.1016/j.rse.2015.12.002.

[164] M. García, S. Saatchi, S. Ustin, and H. Balzter, "Modelling forest canopy height by integrating airborne LiDAR samples with satellite Radar and multispectral imagery," *Int. J. Appl. Earth Observ. Geoinf.*, vol. 66, pp. 159–173, Apr. 2018. doi: 10.1016/j.jag.2017.11.017.

[165] S. Jin, Y. Su, S. Gao, T. Hu, J. Liu, and Q. Guo, "The transferability of random forest in canopy height estimation from multi-source remote sensing data," *Remote Sens.*, vol. 10, no. 8, p. 1183, 2018. doi: 10.3390/rs10081183.

[166] K. Calders, T. Schenkels, H. Bartholomeus, J. Armston, J. Verbesselt, and M. Herold, "Monitoring spring phenology with high temporal resolution terrestrial LiDAR measurements," *Agric. For. Meteorol.*, vol. 203, pp. 158–168, Apr. 2015. doi: 10.1016/j.agrformet.2015.01.009.

[167] Y. Lin and G. West, "Reflecting conifer phenology using mobile terrestrial LiDAR: A case study of Pinus sylvestris growing under the Mediterranean climate in Perth, Australia," *Ecol. Indic.*, vol. 70, pp. 1–9, Nov. 2016. doi: 10.1016/j.ecolind.2016.06.003.

[168] L. Cao et al., "Estimation of forest biomass dynamics in subtropical forests using multi-temporal airborne LiDAR data," *Remote Sens. Environ.*, vol. 178, pp. 158–171, June 2016. doi: 10.1016/j.rse.2016.03.012.

[169] T. Hu et al., "A simple and integrated approach for fire severity assessment using bi-temporal airborne LiDAR data," *Int. J. Appl. Earth Observ. Geoinf.*, vol. 78, pp. 25–38, June 2019. doi: 10.1016/j.jag.2019.01.007.

[170] Y. Su, Q. Guo, B. M. Collins, D. L. Fry, T. Hu, and M. Kelly, "Forest fuel treatment detection using multi-temporal air-

borne lidar data and high-resolution aerial imagery: A case study in the Sierra Nevada Mountains, California," *Int. J. Remote Sens.*, vol. 37, no. 14, pp. 3322–3345, 2016. doi: 10.1080/01431161.2016.1196842.

[171] K. Zhao, J. C. Suarez, M. Garcia, T. Hu, C. Wang, and A. Londo, "Utility of multitemporal lidar for forest and carbon monitoring: Tree growth, biomass dynamics, and carbon flux," *Remote Sens. Environ.*, vol. 204, pp. 883–897, Jan. 2018. doi: 10.1016/j.rse.2017.09.007.

[172] Q. Ma, Y. Su, S. Tao, and Q. Guo, "Quantifying individual tree growth and tree competition using bi-temporal airborne laser scanning data: A case study in the Sierra Nevada Mountains, California," *Int. J. Digit. Earth*, vol. 11, no. 5, pp. 485–503, 2018. doi: 10.1080/17538947.2017.1336578.

[173] M. Bietresato, G. Carabin, R. Vidoni, A. Gasparetto, and F. Mazzetto, "Evaluation of a LiDAR-based 3D-stereoscopic vision system for crop-monitoring applications," *Comput. Electron. Agric.*, vol. 124, pp. 1–13, June 2016. doi: 10.1016/j.compag.2016.03.017.

[174] Y. Lin, "LiDAR: An important tool for next-generation phenotyping technology of high potential for plant phenomics?" *Comput. Electron. Agric.*, vol. 119, no. Suppl. C, pp. 61–73, Nov. 2015. doi: 10.1016/j.compag.2015.10.011.

[175] X. Xiong et al., "Panicle-SEG: A robust image segmentation method for rice panicles in the field based on deep learning and superpixel optimization," *Plant Methods*, vol. 13, no. 1, p. 104, 2017. doi: 10.1186/s13007-017-0254-7.

[176] R. Xu, C. Li, A. Paterson, Y. Jiang, S. Sun, and J. S. Robertson, "Cotton bloom detection using aerial images and convolutional neural network," *Front. Plant Sci.*, vol. 8, p. 2235, Feb. 2017. doi: 10.3389/fpls.2017.02235.

[177] M. P. Pound, A. P. French, J. A. Atkinson, D. M. Wells, M. J. Bennett, and T. Pridmore, "RootNav: Navigating images of complex root architectures," *Plant Physiol.*, vol. 162, no. 4, pp. 1802–1814, 2013. doi: 10.1104/pp.113.221531.

[178] R. Yasrab, J. Atkinson, D. Wells, A. P. French, T. Pridmore, and M. Pound, "RootNav 2.0: Deep Learning for automatic navigation of complex plant root architectures," *GigaScience*, vol. 8, no. 11, p. giz123, 2019. doi: 10.1093/gigascience/giz123.

[179] X. Jin, S. Liu, F. Baret, M. Hemerlé, and A. Comar, "Estimates of plant density of wheat crops at emergence from very low altitude UAV imagery," *Remote Sens. Environ.* vol. 198, pp. 105–114, Sept. 2017. doi: 10.1016/j.rse.2017.06.007.

[180] W. Saeys, B. Lenaerts, G. Craessaerts, and J. De Baerdemaeker, "Estimation of the crop density of small grains using LiDAR sensors," *Biosyst. Eng.*, vol. 102, no. 1, pp. 22–30, 2009. doi: 10.1016/j.biosystemseng.2008.10.003.

[181] F. Perez-Sanz, P. J. Navarro, and M. Egea-Cortines, "Plant phenomics: An overview of image acquisition technologies and image data analysis algorithms," *GigaScience*, vol. 6, no. 11, pp. 1–18, 2017. doi: 10.1093/gigascience/gix092.

[182] H. Wang, W. Zhang, G. Zhou, G. Yan, and N. Clinton, "Image-based 3D corn reconstruction for retrieval of geometrical structural parameters," *Int. J. Remote Sens.*, vol. 30, no. 20, pp. 5505–5513, 2009. doi: 10.1080/01431160903130952.

[183] W. Yang, L. Duan, G. Chen, L. Xiong, and Q. Liu, "Plant phenomics and high-throughput phenotyping: Accelerating rice functional genomics using multidisciplinary technologies," *Curr. Opin. Plant Biol.*, vol. 16, no. 2, pp. 180–187, 2013. doi: 10.1016/j.pbi.2013.03.005.

[184] S. Crommelinck and B. Höfle, "Simulating an autonomously operating low-cost static terrestrial LiDAR for multitemporal maize crop height measurements," *Remote Sens.*, vol. 8, no. 3, p. 205, 2016. doi: 10.3390/rs8030205.

[185] Q. Guo et al., "Crop 3D: A platform based on LiDAR for 3D high-throughput crop phenotyping," *Scientia Sinica Vitae*, vol. 46, no. 10, pp. 1210–1221, 2016. doi: 10.1007/s11427-017-9056-0.

[186] S. Madec et al., "High-throughput phenotyping of plant height: Comparing unmanned aerial vehicles and ground LiDAR estimates," *Front. Plant Sci.*, vol. 8, p. 2002, Nov. 2017. doi: 10.3389/fpls.2017.02002.

[187] J. D. C. Walter, J. Edwards, G. McDonald, and H. Kuchel, "Estimating biomass and canopy height with LiDAR for field crop breeding," *Frontiers Plant Sci.*, vol. 10, p. 1145, Sept. 2019. doi: 10.3389/fpls.2019.01145.

[188] W. Su, J. Zhan, M. Zhang, and D. Wu, "Estimation method of crop leaf area index based on airborne LiDAR data," *Trans. Chin. Soc. Agric. Mach.*, vol. 47, no. 3, pp. 272–277, 2016. doi: 10.6041/j.issn.1000-1298.2016.03.038.

[189] J. ten Harkel, H. Bartholomeus, and L. Kooistra, "Biomass and crop height estimation of different crops using UAV-based lidar," *Remote Sens.*, vol. 12, no. 1, p. 17, 2020. doi: 10.3390/rs12010017.

[190] J. A. Jimenez-Berni et al., "High throughput determination of plant height, ground cover, and above-ground biomass in wheat with LiDAR," *Front. Plant Sci.*, vol. 9, p. 237, Feb. 2018. doi: 10.3389/fpls.2018.00237.

[191] O. Mohamad, O. Suhaimi, and M. Abdullah, "The relationships between harvest index, grain yield and biomass in rice," *MARDI Res. J.*, vol. 22, no. 1, pp. 29–34, 1994.

[192] Y. Su et al., "Evaluating maize phenotype dynamics under drought stress using terrestrial lidar," *Plant Methods*, vol. 15, no. 1, pp. 11–26, 2019. doi: 10.1186/s13007-019-0396-x.

[193] J. T. Heun et al., "Deployment of lidar from a ground platform: Customizing a low-cost, information-rich and user-friendly application for field phenomics research," *Sensors*, vol. 19, no. 24, p. 5358, 2019. doi: 10.3390/s19245358.

[194] L. Du et al., "Potential of spectral ratio indices derived from hyperspectral LiDAR and laser-induced chlorophyll fluorescence spectra on estimating rice leaf nitrogen contents," *Opt. Express*, vol. 25, no. 6, pp. 6539–6549, 2017. doi: 10.1364/OE.25.006539.

[195] J. U. Eitel, T. S. Magney, L. A. Vierling, T. T. Brown, and D. R. Huggins, "LiDAR based biomass and crop nitrogen estimates for rapid, non-destructive assessment of wheat nitrogen status," *Field Crops Res.*, vol. 159, pp. 21–32, Mar. 2014. doi: 10.1016/j.fcr.2014.01.008.

[196] S. Yang, Z. Xue, L. Zhang, H. Su, and S. Zhou, "Fusion of hyperspectral and LiDAR data: A case study for refined crop classification in agricultural region of Zhangye Oasis in the middle reaches of Heihe River," *Remote Sens. Land Resour.*, vol. 30, no. 4, pp. 33–40, 2018. doi: 10.6046/gtzyyg.2018.04.06.

[197] K. E. Anderson et al., "Estimating vegetation biomass and cover across large plots in shrub and grass dominated drylands

using terrestrial lidar and machine learning," *Ecol. Indic.*, vol. 84, pp. 793–802, Jan. 2018. doi: 10.1016/j.ecolind.2017.09.034.

[198] S. Cooper, D. Roy, C. Schaaf, and I. Paynter, "Examination of the potential of terrestrial laser scanning and structure-from-motion photogrammetry for rapid nondestructive field measurement of grass biomass," *Remote Sens.*, vol. 9, no. 6, p. 531, 2017. doi: 10.3390/rs9060531.

[199] K. Xu et al. "Estimation of degraded grassland aboveground biomass using machine learning methods from terrestrial laser scanning data," *Ecol. Indic.*, vol. 108, p. 105,747, Jan. 2020. doi: 10.1016/j.ecolind.2019.105747.

[200] M. E. Hajj et al., "Soil moisture retrieval over irrigated grassland using X-band SAR data," *Remote Sens. Environ.*, vol. 176, pp. 202–218, Apr. 2016. doi: 10.1016/j.rse.2016.01.027.

[201] V. S. Jansen, C. A. Kolden, and H. J. Schmalz, "The development of near real-time biomass and cover estimates for adaptive rangeland management using Landsat 7 and Landsat 8 surface reflectance products," *Remote Sens.*, vol. 10, no. 7, p. 22, July 2018. doi: 10.3390/rs10071057.

[202] S. Mermoz, T. Thuy Le, L. Villard, M. Réjou-Méchain, and J. Seifert-Granzin, "Biomass assessment in the Cameroon savanna using ALOS PALSAR data," *Remote Sens. Environ.*, vol. 155, pp. 109–119, Dec. 2014. doi: 10.1016/j.rse.2014.01.029.

[203] J. J. Mitchell, N. F. Glenn, T. T. Sankey, W. R. Derryberry, R. C. Hruska, and M. O. Anderson, "Small-footprint lidar estimations of sagebrush canopy characteristics," *Photogramm. Eng. Remote Sens.*, vol. 77, no. 5, pp. 521–530, May, 2011. doi: 10.14358/PERS.77.5.521.

[204] H. E. Greaves et al., "Estimating aboveground biomass and leaf area of low-stature Arctic shrubs with terrestrial LiDAR," *Remote Sens. Environ.*, vol. 164, pp. 26–35, July 2015. doi: 10.1016/j.rse.2015.02.023.

[205] H. E. Greaves et al., "High-resolution mapping of aboveground shrub biomass in Arctic tundra using airborne lidar and imagery," *Remote Sens. Environ.*, vol. 184, pp. 361–373, Oct. 2016. doi: 10.1016/j.rse.2016.07.026.

[206] H. E. Greaves et al., "Applying terrestrial lidar for evaluation and calibration of airborne lidar-derived shrub biomass estimates in Arctic tundra," *Remote Sens. Lett.*, vol. 8, no. 2, pp. 175–184, 2016. doi: 10.1080/2150704X.2016.1246770.

[207] D. R. Streutker and N. F. Glenn, "LiDAR measurement of sagebrush steppe vegetation heights," *Remote Sens. Environ.*, vol. 102, nos. 1–2, pp. 135–145, 2006. doi: 10.1016/j.rse.2006.02.011.

[208] M. T. Schaefer and D. W. Lamb, "A combination of plant NDVI and LiDAR measurements improve the estimation of pasture biomass in tall fescue (Festuca arundinacea var. Fletcher)," *Remote Sens.*, vol. 8, no. 2, p. 10, 2016. doi: 10.3390/rs8020109.

[209] J. Wijesingha, T. Moeckel, F. Hensgen, and M. Wachendorf, "Evaluation of 3D point cloud-based models for the prediction of grassland biomass," *Int. J. Appl. Earth Observ. Geoinf.*, vol. 78, pp. 352–359, June 2019. doi: 10.1016/j.jag.2018.10.006.

[210] D. Schulze-Brüninghoff, F. Hensgen, M. Wachendorf, et al. "Methods for LiDAR-based estimation of extensive grassland biomass," *Comput. Electron.s Agriculture*, vol. 156, pp. 693–699, 2019. doi: 10.1016/j.compag.2018.11.041]

[211] D. Wang, X. Xin, Q. Shao, and T. Astor, "Modeling aboveground biomass in hulunber grassland ecosystem by using unmanned aerial vehicle discrete lidar," *Sensors*, vol. 17, no. 12, p. 180, 2017. doi: 10.3390/s17010180.

[212] B. Reddersen, T. Fricke, and M. Wachendorf, "A multi-sensor approach for predicting biomass of extensively managed grassland," *Comput. Electron. Agric.*, vol. 109, pp. 247–260, Nov. 2014. doi: 10.1016/j.compag.2014.10.011.

[213] N. R. Goodwin, N. C. Coops, T. R. Tooke, J. A. Vooght, and R. Tooke, "Characterizing urban surface cover and structure with airborne lidar technology," *Can. J. Remote Sens.*, vol. 35, no. 3, pp. 297–309, 2009. doi: 10.5589/m09-015.

[214] W. Y. Yan, A. Shaker, and N. El-Ashmawy, "Urban land cover classification using airborne LiDAR data: A review," *Remote Sens. Environ*. vol. 158, pp. 295–310, Mar. 2015. doi: 10.1016/j.rse.2014.11.001.

[215] Y. Zhao, Q. Hu, H. Li, S. Wang, and M. Ai, "Evaluating carbon sequestration and PM2.5 removal of urban street trees using mobile laser scanning data," *Remote Sens.*, vol. 10, no. 11, p. 1759, 2018. doi: 10.3390/rs10111759.

[216] J. Zhang, Q. Sun, Z. Ye, and X. Chen, "New technology for ecological remote sensing: Light, small unmanned aerial vehicles (UAV)," *Tropic. Geogr.*, vol. 39, no. 4, pp. 604–615, 2019.

[217] A. P. Charaniya, R. Manduchi, and S. Lodha, "Supervised parametric classification of aerial LiDAR data," in *Proc. 2004 Conf. Comput. Vis. Pattern Recognit. Workshop*, Washington D. C., pp. 30–30. doi: 10.1109/CVPR.2004.446.

[218] M.-J. Huang, S.-W. Shyue, L.-H. Lee, and C-C. Kao "A knowledge-based approach to urban feature classification using aerial imagery with lidar data," *Photogramm. Eng. Remote Sens.* vol. 74, no. 12, pp. 1473–1485, 2008. doi: 10.14358/PERS.74.12.1473.

[219] N. Q. Minh and L. P. Hien, "Land cover classification using LiDAR intensity data and neural network," *J. Korean Soc. Surv., Geodesy, Photogramm., Cartogr.*, vol. 29, no. 4, pp. 429–438, 2011. doi: 10.7848/ksgpc.2011.29.4.429.

[220] J. Niemeyer, J. D. Wegner, C. Mallet, F. Rottensteiner, and U. Soergel, "Conditional random fields for urban scene classification with full waveform LiDAR data," in *Proc. Photogramm. Image Anal. - ISPRS Conf.*, 2011. doi: 10.1007/978-3-642-24393-6_20.

[221] F. Samadzadegan, B. Bigdeli, and P. Ramzi, "A multiple classifier system for classification of LIDAR remote sensing data using multi-class SVM," in *Multiple Classifier Systems, Proceedings, Lecture Notes in Computer Science*, N. El Gayar, J. Kittler, and F. Roli, Eds. Berlin: Springer-Verlag, 2010, pp. 254–263.

[222] H. Wei, and Bartels, "Unsupervised segmentation using gabor wavelets and statistical features in LIDAR data analysis," in *Proc. 18th Int. Conf. Pattern Recognit. (ICPR'06)*, Hongkong, China, 2006, pp. 667–670. doi: 10.1109/ICPR.2006.1145.

[223] S. Xu, S. Xu, N. Ye, and F. Zhu, "Automatic extraction of street trees' nonphotosynthetic components from MLS data," *Int. J. Appl. Earth Observ. Geoinf.*, vol. 69, pp. 64–77, July 2018. doi: 10.1016/j.jag.2018.02.016.

[224] M. Alonzo, B. Bookhagen, and D. A. Roberts, "Urban tree species mapping using hyperspectral and lidar data fusion,"

Remote Sens. Environ., vol. 148, pp. 70–83, May 2014. doi: 10.1016/j.rse.2014.03.018.

[225] A. Borcs and C. Benedek, "Extraction of vehicle groups in airborne lidar point clouds with two-level point processes," *IEEE Trans. Geosci. Remote Sens.*, vol. 53, no. 3, pp. 1475–1489, 2015. doi: 10.1109/TGRS.2014.2344438.

[226] T. Sasaki, J. Imanishi, K. Ioki, Y. Morimoto, and K. Kitada, "Object-based classification of land cover and tree species by integrating airborne LiDAR and high spatial resolution imagery data," *Landscape Ecol. Eng.*, vol. 8, no. 2, pp. 157–171, 2012. doi: 10.1007/s11355-011-0158-z.

[227] B. Höfle, M. Hollaus, and J. Hagenauer, "Urban vegetation detection using radiometrically calibrated small-footprint full-waveform airborne LiDAR data," *ISPRS J. Photogramm. Remote Sens.*, vol. 67, pp. 134–147, Jan. 2012. doi: 10.1016/j.isprsjprs.2011.12.003.

[228] C. Zhang, Y. Zhou, and F. Qiu, "Individual tree segmentation from LiDAR point clouds for urban forest inventory," *Remote Sens.*, vol. 7, no. 6, pp. 7892–7913, 2015. doi: 10.3390/rs70607892.

[229] X. Hu, Y. Li, J. Shan, J. Zhang, and Y. Zhang, "Road centerline extraction in complex urban scenes from LiDAR data based on multiple features," *IEEE Trans. Geosci. Remote Sens.*, vol. 52, no. 11, pp. 7448–7456, 2014. doi: 10.1109/TGRS.2014.2312793.

[230] S. W. MacFaden, J. P. M. O'Neil-Dunne, A. R. Royar, J. T. W. Lu, and A. Rundle, "High-resolution tree canopy mapping for New York City using LIDAR and object-based image analysis," *J. Appl. Remote Sens.*, vol. 6, no. 1, pp. 063567, 2012. doi: 10.1117/1.JRS.6.063567.

[231] J. P. M. O'Neil-Dunne, S. W. MacFaden, A. R. Royar, and K. C. Pelletier, "An object-based system for LiDAR data fusion and feature extraction," *Geocarto Int.*, vol. 28, no. 3, pp. 227–242, 2013. doi: 10.1080/10106049.2012.689015.

[232] M. Soilán, B. Riveiro, J. Martínez-Sánchez, and P. Arias, "Traffic sign detection in MLS acquired point clouds for geometric and image-based semantic inventory," *ISPRS J. Photogramm. Remote Sens.*, vol. 114, pp. 92–101, Apr. 2016. doi: 10.1016/j.isprsjprs.2016.01.019.

[233] W. Xiao, B. Vallet, K. Schindler, and N. Paparoditis, "Street-side vehicle detection, classification and change detection using mobile laser scanning data," *ISPRS J. Photogramm. Remote Sens.*, vol. 114, pp. 166–178, Apr. 2016. doi: 10.1016/j.isprsjprs.2016.02.007.

[234] W. Zhou, "An object-based approach for urban land cover classification: Integrating LiDAR height and intensity data," *IEEE Geosci. Remote Sens. Lett.*, vol. 10, no. 4, pp. 928–931, 2013. doi: 10.1109/LGRS.2013.2251453.

[235] J. Niemeyer, F. Rottensteiner, and U. Soergel, "Contextual classification of lidar data and building object detection in urban areas," *ISPRS J. Photogramm.y Remote Sens.*, vol. 87, pp. 152–165, Jan. 2014. doi: 10.1016/j.isprsjprs.2013.11.001.

[236] G. Vosselman, M. Coenen, and F. Rottensteiner, "Contextual segment-based classification of airborne laser scanner data," *ISPRS J. Photogramm. Remote Sens.*, vol. 128, pp. 354–371, June 2017. doi: 10.1016/j.isprsjprs.2017.03.010.

[237] S. Xu, G. Vosselman, and S. Oude Elberink, "Multiple-entity based classification of airborne laser scanning data in urban areas," *ISPRS J. Photogramm. Remote Sens.*, vol. 88, pp. 1–15, Feb. 2014. doi: 10.1016/j.isprsjprs.2013.11.008.

[238] Y. Sun, X. Zhang, X. Zhao, and Q. Xin, "Extracting building boundaries from high resolution optical images and LiDAR data by integrating the convolutional neural network and the active contour model," *Remote Sens.*, vol. 10, no. 9, p. 1459, 2018. doi: 10.3390/rs10091459.

[239] V. Giannico, R. Lafortezza, R. John, G. Sanesi, L. Pesola, and J. Chen, "Estimating stand volume and above-ground biomass of urban forests using LiDAR," *Remote Sens.*, vol. 8, no. 4, 2016. doi: 10.3390/rs8040339.

[240] L. M. Moskal, D. M. Styers, and M. Halabisky, "Monitoring urban tree cover using object-based image analysis and public domain remotely sensed data," *Remote Sens.*, vol. 3, no. 10, pp. 2243–2262, 2011. doi: 10.3390/rs3102243.

[241] J. J. Richardson, L. M. Moskal, and S.-H. Kim, "Modeling approaches to estimate effective leaf area index from aerial discrete-return LIDAR," *Agric. For. Meteorol.*, vol. 149, nos. 6–7, pp. 1152–1160, 2009. doi: 10.1016/j.agrformet.2009.02.007.

[242] J. Susaki, Y. Komiya, and K. Takahashi, "Calculation of enclosure Index for assessing urban landscapes using digital surface models," *IEEE J. Sel. Topics Appl. Earth Observ. Remote Sens.*, vol. 7, no. 10, pp. 4038–4045, 2014. doi: 10.1109/JSTARS.2013.2271380.

[243] M. Alonzo, B. Bookhagen, J. P. McFadden, A. Sun, and D. A. Roberts, "Mapping urban forest leaf area index with airborne lidar using penetration metrics and allometry," *Remote Sens. Environ.*, vol. 162, pp. 141–153, June 2015. doi: 10.1016/j.rse.2015.02.025.

[244] R. J. C. Caynes, M. G. E. Mitchell, D. S. Wu, K. Johansen, and J. R. Rhodes, "Using high-resolution LiDAR data to quantify the three-dimensional structure of vegetation in urban green space," *Urban Ecosyst.*, vol. 19, no. 4, pp. 1749–1765, 2016. doi: 10.1007/s11252-016-0571-z.

[245] G. Matasci, N. C. Coops, D. A. Williams, and N. Page, "Mapping tree canopies in urban environments using airborne laser scanning (ALS): a Vancouver case study," *For. Ecosyst.*, vol. 5, no. 1, p. 31, 2018. doi: 10.1186/s40663-018-0146-y.

[246] C. M. Chance, N. C. Coops, A. A. Plowright, T. R. Tooke, A. Christen, and N. Aven, "Invasive shrub mapping in an urban environment from hyperspectral and LiDAR-derived attributes," *Front. Plant Sci.*, vol. 7, p. 1528, 2016. doi: 10.3389/fpls.2016.01528.

[247] S. Yu et al., "View-based greenery: A three-dimensional assessment of city buildings' green visibility using Floor Green View Index," *Landscape Urban Plan.*, vol. 152, pp. 13–26, Aug. 2016. doi: 10.1016/j.landurbplan.2016.04.004.

[248] B. Bonczak and C. E. Kontokosta, "Large-scale parameterization of 3D building morphology in complex urban landscapes using aerial LiDAR and city administrative data," *Comput. Environ. Urban Syst.*, vol. 73, pp. 126–142, Jan. 2019. doi: 10.1016/j.compenvurbsys.2018.09.004.

[249] P. Dorninger and N. Pfeifer, "A comprehensive automated 3D approach for building extraction, reconstruction, and regularization from airborne laser scanning point clouds," *Sensors*, vol. 8, no. 11, pp. 7323–7343, 2008. doi: 10.3390/s8117323.

[250] C. Kidd and L. Chapman, "Derivation of sky-view factors from lidar data," *Int. J. Remote Sens.*, vol. 33, no. 11, pp. 3640–3652, 2012. doi: 10.1080/01431161.2011.635163.

[251] A. Sampath and S. Jie, "Segmentation and reconstruction of polyhedral building roofs from aerial Lidar point clouds," *IEEE Trans. Geosci. Remote Sens.*, vol. 48, no. 3, pp. 1554–1567, 2010. doi: 10.1109/TGRS.2009.2030180.

[252] S. Xia and R. Wang, "Extraction of residential building instances in suburban areas from mobile LiDAR data," *ISPRS J. Photogramm. Remote Sens.*, vol. 144, pp. 453–468, Oct. 2018. doi: 10.1016/j.isprsjprs.2018.08.009.

[253] D. Van der Zande, J. Stuckens, W. W. Verstraeten, S. Mereu, B. Muys, and P. Coppin, "3D modeling of light interception in heterogeneous forest canopies using ground-based LiDAR data," *Int. J. Appl. Earth Observ. Geoinf.*, vol. 13, no. 5, pp. 792–800, 2011. doi: 10.1016/j.jag.2011.05.005.

[254] M. T. Lamelas-Gracia, D. Riaño, and S. Ustin, "A LiDAR signature library simulated from 3-dimensional Discrete Anisotropic Radiative Transfer (DART) model to classify fuel types using spectral matching algorithms," *GISci. Remote Sens.*, vol. 56, no. 7, pp. 988–1023, 2019. doi: 10.1080/15481603.2019.1601805.

[255] F. D. Schneider et al., "Simulating imaging spectrometer data: 3D forest modeling based on LiDAR and in situ data," *Remote Sens. Environ.*, vol. 152, no. 9, pp. 235–250, 2014. doi: 10.1016/j.rse.2014.06.015.

[256] Y. Su et al., "Large-scale geographical variations and climatic controls on crown architecture traits," *J. Geophys. Res., Biogeosci.*, vol. 125, no. 2, p. e2019JG005306, 2020. doi: 10.1029/2019JG005306.

[257] S. Tao, Q. Guo, C. Li, Z. Wang, and J. Fang, "Global patterns and determinants of forest canopy height," *Ecology*, vol. 97, no. 12, pp. 3265–3270, 2016. doi: 10.1002/ecy.1580.

[258] B.-L. Xue et al., "Global patterns of woody residence time and its influence on model simulation of aboveground biomass," *Glob. Biogeochem. Cycles*, vol. 31, no. 5, pp. 821–835, 2017. doi: 10.1002/2016GB005557.

[259] K. M. Bergen et al., "Remote sensing of vegetation 3-D structure for biodiversity and habitat: Review and implications for lidar and radar spaceborne missions," *J. Geophys. Res., Biogeosci.*, vol. 114, no. G2, p. G00E06, 2009. doi: 10.1029/2008JG000883.

[260] M. Kearney and W. Porter, "Mechanistic niche modelling: Combining physiological and spatial data to predict species' ranges," *Ecol. Lett.*, vol. 12, no. 4, pp. 334–350, 2009. doi: 10.1111/j.1461-0248.2008.01277.x.

[261] F. Zhao, R. A. Sweitzer, Q. Guo, and M. Kelly, "Characterizing habitats associated with fisher den structures in the Southern Sierra Nevada, California using discrete return lidar," *For. Ecol. Manage.*, vol. 280, pp. 112–119, Sept. 2012. doi: 10.1016/j.foreco.2012.06.005.

[262] C. García-Feced, D. J. Tempel, and M. Kelly, "LiDAR as a tool to characterize wildlife habitat: California spotted owl nesting habitat as an example," *J. For.*, vol. 109, no. 8, pp. 436–443, 2011.

[263] M. P. North et al., "Cover of tall trees best predicts California spotted owl habitat," *For. Ecol. Manage.*, vol. 405, pp. 166–178, Dec. 2017. doi: 10.1016/j.foreco.2017.09.019.

[264] S. R. Loarie, C. J. Tambling, and G. P. Asner, "Lion hunting behaviour and vegetation structure in an African savanna," *Anim. Behav.*, vol. 85, no. 5, pp. 899–906, 2013. doi: 10.1016/j.anbehav.2013.01.018.

[265] R. V. Blakey, B. S. Law, R. T. Kingsford, and J. Stoklosa, "Terrestrial laser scanning reveals below-canopy bat trait relationships with forest structure," *Remote Sens. Environ.*, vol. 198, pp. 40–51, Sept. 2017. doi: 10.1016/j.rse.2017.05.038.

[266] M. P. Eichhorn, J. Ryding, M. J. Smith, R. M. A. Gill, G. M. Siriwardena, and R. J. Fuller, "Effects of deer on woodland structure revealed through terrestrial laser scanning," *J. Appl. Ecol.*, vol. 54, no. 6, pp. 1615–1626, 2017. doi: 10.1111/1365-2664.12902.

[267] N. C. Coops et al., "A forest structure habitat index based on airborne laser scanning data," *Ecol. Indic.*, vol. 67, pp. 346–357, Aug. 2016. doi: 10.1016/j.ecolind.2016.02.057.

[268] A. Hastings, J. Clifton-Brown, M. Wattenbach, C. P. Mitchell, and P. Smith, "The development of MISCANFOR, a new Miscanthus crop growth model: Towards more robust yield predictions under different climatic and soil conditions," *Global Change Biol. Bioenergy*, vol. 1, no. 2, pp. 154–170, 2009. doi: 10.1111/j.1757-1707.2009.01007.x.

[269] I. R. Johnson and J. H. M. Thornley, "Vegetative crop growth model incorporating leaf area expansion and senescence, and applied to grass," *Plant, Cell Environ.*, vol. 6, no. 9, pp. 721–729, 1983. doi: 10.1111/j.1365-3040.1983.tb01190.x.

[270] L. Cabrera-Bosquet, J. Crossa, J. v Zitzewitz, M. D. Serret, and J. L. Araus, "High-throughput phenotyping and genomic selection: The frontiers of crop breeding converge," *J. Integr. Plant Biol.*, vol. 54, no. 5, pp. 312–320, 2012. doi: 10.1111/j.1744-7909.2012.01116.x.

[271] S. Liu, P. Martre, S. Buis, M. Abichou, B. Andrieu, and F. Baret, "Estimation of plant and canopy architectural traits using the digital plant phenotyping platform," *Plant Physiol.*, vol. 181, no. 3, pp. 881–890, 2019. doi: 10.1104/pp.19.00554.

[272] J. Lopatin, K. Dolos, H. J. Hernández, M. Galleguillos, and F. E. Fassnacht, "Comparing generalized linear models and random forest to model vascular plant species richness using LiDAR data in a natural forest in central Chile," *Remote Sens. Environ.*, vol. 173, pp. 200–210, Feb. 2016. doi: 10.1016/j.rse.2015.11.029.

[273] V. S. Jansen, C. A. Kolden, H. E. Greaves, and J. U. H. Eitel, "Lidar provides novel insights into the effect of pixel size and grazing intensity on measures of spatial heterogeneity in a native bunchgrass ecosystem," *Remote Sens. Environ.*, vol. 235, p. 111,432, Dec. 2019. doi: 10.1016/j.rse.2019.111432.

[274] J. E. Moeslund et al., "Light detection and ranging explains diversity of plants, fungi, lichens, and bryophytes across multiple habitats and large geographic extent," *Ecol. Appl.*, vol. 29, no. 5, p. e01907, 2019. doi: 10.1002/eap.1907.

[275] A. Marcinkowska-Ochtyra, A. Jarocińska, K. Bzdęga, and B. Tokarska-Guzik, "Classification of expansive grassland species in different growth stages based on hyperspectral and LiDAR data," *Remote Sens.*, vol. 10, no. 12, p. 2019, 2018. doi: 10.3390/rs10122019.

[276] R. J. Fisher, B. Sawa, and B. Prieto, "A novel technique using LiDAR to identify native-dominated and tame-dominated grass-

lands in Canada," *Remote Sens. Environ.*, vol. 218, pp. 201–206, Dec. 2018. doi: 10.1016/j.rse.2018.10.003.

[277] E. A. Gage and D. J. Cooper, "Relationships between landscape pattern metrics, vertical structure and surface urban heat island formation in a Colorado suburb," *Urban Ecosyst.*, vol. 20, no. 6, pp. 1229–1238, 2017. doi: 10.1007/s11252-017-0675-0.

[278] F. Lindberg and C. S. B. Grimmond, "Nature of vegetation and building morphology characteristics across a city: Influence on shadow patterns and mean radiant temperatures in London," *Urban Ecosyst.*, vol. 14, no. 4, pp. 617–634, 2011. doi: 10.1007/s11252-011-0184-5.

[279] L. S. Rose and R. Levinson, "Analysis of the effect of vegetation on albedo in residential areas: Case studies in suburban Sacramento and Los Angeles, CA," *GISci. Remote Sens.*, vol. 50, no. 1, pp. 64–77, 2013. doi: 10.1080/15481603.2013.778557.

[280] T. R. Tooke, N. C. Coops, J. A. Voogt, and M. J. Meitner, "Tree structure influences on rooftop-received solar radiation," *Landscape Urban Plan.*, vol. 102, no. 2, pp. 73–81, 2011. doi: 10.1016/j.landurbplan.2011.03.011.

[281] B. Yu, H. Liu, J. Wu, and W-M. Lin, "Investigating impacts of urban morphology on spatio-temporal variations of solar radiation with airborne LIDAR data and a solar flux model: a case study of downtown Houston," *Int. J. Remote Sens.*, vol. 30, no. 17, pp. 4359–4385, 2009. doi: 10.1080/01431160802555846.

[282] B. Guinot, J.-C. Roger, H. Cachier, W. Pucai, B. Jianhui, and Y. Tong, "Impact of vertical atmospheric structure on Beijing aerosol distribution," *Atmos. Environ.*, vol. 40, no. 27, pp. 5167–5180, 2006. doi: 10.1016/j.atmosenv.2006.03.051.

[283] Y. Tian, W. Zhou, Y. Qian, Z. Zheng, and J. Yan, "The effect of urban 2D and 3D morphology on air temperature in residential neighborhoods," *Landscape Ecol.*, vol. 34, no. 5, pp. 1161–1178, 2019. doi: 10.1007/s10980-019-00834-7.

[284] Q. Zhao, S. W. Myint, E. A. Wentz, and C. Fan, "Rooftop surface temperature analysis in an urban residential environment," *Remote Sens.*, vol. 7, no. 9, pp. 12,135–12,159, 2015. doi: 10.3390/rs70912135.

[285] F. Kong et al., "Retrieval of three-dimensional tree canopy and shade using terrestrial laser scanning (TLS) data to analyze the cooling effect of vegetation," *Agric. For. Meteorol.*, vol. 217, pp. 22–34, Feb. 2016. doi: 10.1016/j.agrformet.2015.11.005.

[286] A. A. Plowright, N. C. Coops, C. M. Chance, S. R. J. Sheppard, and N. W. Aven, "Multi-scale analysis of relationship between imperviousness and urban tree height using airborne remote sensing," *Remote Sens. Environ.*, vol. 194, pp. 391–400, June 2017. doi: 10.1016/j.rse.2017.03.045.

[287] T. Sasaki, J. Imanishi, W. Fukui, and Y. Morimoto, "Fine-scale characterization of bird habitat using airborne LiDAR in an urban park in Japan," *Urban For. Urban Green.*, vol. 17, pp. 16–22, June 2016. doi: 10.1016/j.ufug.2016.03.007.

[288] K. I. Landau and W. J. van Leeuwen, "Fine scale spatial urban land cover factors associated with adult mosquito abundance and risk in Tucson, Arizona," *J. Vector Ecol.*, vol. 37, no. 2, pp. 407–418, 2012. doi: 10.1111/j.1948-7134.2012.00245.x.

[289] R. Pecero-Casimiro et al., "Urban aerobiological risk mapping of ornamental trees using a new index based on LiDAR and Kriging: A case study of plane trees," *Sci. Total Environ.*, vol. 693, p. 133,576, Nov. 2019. doi: 10.1016/j.scitotenv.2019.07.382.

[290] K. A. Hartfield, K. I. Landau, and W. J. D. v Leeuwen, "Fusion of high resolution aerial multispectral and LiDAR data: Land cover in the context of urban mosquito habitat," *Remote Sens.*, vol. 3, no. 11, pp. 2364–2383, 2011. doi: 10.3390/rs3112364.

[291] T. J. Fewtrell, A. Duncan, C. C. Sampson, J. C. Neal, and P. D. Bates, "Benchmarking urban flood models of varying complexity and scale using high resolution terrestrial LiDAR data," *Phys. Chem. Earth, A/B/C*, vol. 36, nos. 7–8, pp. 281–291, 2011. doi: 10.1016/j.pce.2010.12.011.

[292] Y. Ju et al., "Erratum to: Planning for the change: Mapping sea level rise and storm inundation in Sherman Island Using 3Di Hydrodynamic Model and LiDAR," in *Seeing Cities Through Big Data: Research, Methods and Applications in Urban Informatics, Springer Geography*, P. V. Thakuriah, N. Tilahun and M. Zellner, Eds. Cham: Springer-Verlag, 2017, pp. E1–E1.

[293] S. Ortega, A. Trujillo, J. M. Santana, J. P. Suárez, and J. Santana, "Characterization and modeling of power line corridor elements from LiDAR point clouds," *ISPRS J. Photogramm. Remote Sens.*, vol. 152, pp. 24–33, June 2019. doi: 10.1016/j.isprsjprs.2019.03.021.

[294] T. R. Tooke, M. van der Laan, and N. C. Coops, "Mapping demand for residential building thermal energy services using airborne LiDAR," *Appl. Energy*, vol. 127, pp. 125–134, Aug. 2014. doi: 10.1016/j.apenergy.2014.03.035.

[295] J. Yang and Z. Kang, "Voxel-Based Extraction of Transmission Lines From Airborne LiDAR Point Cloud Data," *IEEE J. Sel. Topics Appl. Earth Observ. Remote Sens.*, vol. 11, no. 10, pp. 3892–3904, 2018. doi: 10.1109/JSTARS.2018.2869542.

[296] A. G. Kashani, M. J. Olsen, C. E. Parrish, and N. Wilson, "A review of LiDAR radiometric processing: From ad hoc intensity correction to rigorous radiometric calibration," *Sensors*, vol. 15, no. 11, pp. 28,099–28,128, 2015. doi: 10.3390/s151128099.

[297] B. Höfle and N. Pfeifer, "Correction of laser scanning intensity data: Data and model-driven approaches," *ISPRS J. Photogramm. Remote Sens.*, vol. 62, no. 6, pp. 415–433, 2007. doi: 10.1016/j.isprsjprs.2007.05.008.

[298] S. Kaasalainen et al., "Radiometric calibration of LIDAR intensity with commercially available reference targets," *IEEE Trans. Geosci. Remote Sens.*, vol. 47, no. 2, pp. 588–598, 2009. doi: 10.1109/TGRS.2008.2003351.

[299] A. Vain, X. Yu, S. Kaasalainen, and J. Hyyppa, "Correcting airborne laser scanning intensity data for automatic gain control effect," *IEEE Geosci. Remote Sens. Lett.*, vol. 7, no. 3, pp. 511–514, 2010. doi: 10.1109/LGRS.2010.2040578.

[300] W. Y. Yan, A. Shaker, A. Habib, and A. P. Kersting, "Improving classification accuracy of airborne LiDAR intensity data by geometric calibration and radiometric correction," *ISPRS J. Photogramm. Remote Sens.*, vol. 67, pp. 35–44, Jan. 2012. doi: 10.1016/j.isprsjprs.2011.10.005.

[301] P. J. Hartzell, C. L. Glennie, and D. C. Finnegan, "Empirical waveform decomposition and radiometric calibration of a terrestrial full-waveform laser scanner," *IEEE Trans. Geosci. Remote Sens.*, vol. 53, no. 1, pp. 162–172, 2014. doi: 10.1109/TGRS.2014.2320134.

[302] E. S. Douglas et al., "Finding leaves in the forest: The dual-wavelength Echidna lidar," *IEEE Geosci. Remote Sens. Lett.*, vol. 12, no. 4, pp. 776–780, 2014. doi: 10.1109/LGRS.2014.2361812.

[303] S. Hancock, P. Lewis, M. Foster, M. Disney, and J. P. Muller, "Measuring forests with dual wavelength lidar: A simulation study over topography," *Agric. For. Meteorol.*, vol. 161, pp. 123–133, Aug. 2012. doi: 10.1016/j.agrformet.2012.03.014.

[304] F. Morsdorf, C. Nichol, T. Malthus, and I. H. Woodhouse, "Assessing forest structural and physiological information content of multi-spectral LiDAR waveforms by radiative transfer modelling," *Remote Sens. Environ.*, vol. 113, no. 10, pp. 2152–2163, 2009. doi: 10.1016/j.rse.2009.05.019.

[305] M. Kukkonen, M. Maltamo, L. Korhonen, and P. Packalen, "Multispectral airborne LiDAR data in the prediction of boreal tree species composition," *IEEE Trans. Geosci. Remote Sens.*, vol. 57, no. 6, pp. 3462–3471, 2019. doi: 10.1109/TGRS.2018.2885057.

[306] S. Luo et al., "Fusion of airborne LiDAR data and hyperspectral imagery for aboveground and belowground forest biomass estimation," *Ecol. Indic.*, vol. 73, pp. 378–387, Feb. 2017. doi: 10.1016/j.ecolind.2016.10.001.

[307] T. Sankey, J. Donager, J. McVay, and J. V. Sankey, "UAV lidar and hyperspectral fusion for forest monitoring in the southwestern USA," *Remote Sens. Environ.*, vol. 195, pp. 30–43, June 2017. doi: 10.1016/j.rse.2017.04.007.

[308] A. Swatantran, R. Dubayah, D. Roberts, M. Hofton, and J. B. Blair, "Mapping biomass and stress in the Sierra Nevada using lidar and hyperspectral data fusion," *Remote Sens. Environ.*, vol. 115, no. 11, pp. 2917–2930, Nov. 2011. doi: 10.1016/j.rse.2010.08.027.

[309] N. C. Coops, F. Morsdorf, M. E. Schaepman, and N. E. Zimmermann, "Characterization of an alpine tree line using airborne LiDAR data and physiological modeling," *Glob. Change Biol.*, vol. 19, no. 12, pp. 3808–3821, 2013. doi: 10.1111/gcb.12319.

[310] J. S. Deems, T. H. Painter, and D. C. Finnegan, "Lidar measurement of snow depth: A review," *J. Glaciol.*, vol. 59, no. 215, pp. 467–479, 2013. doi: 10.3189/2013JoG12J154.

[311] Z. Zheng, Q. Ma, S. Jin, Y. Su, Q. Guo, and R. C. Bales, "Canopy and Terrain Interactions Affecting Snowpack Spatial Patterns in the Sierra Nevada of California," *Water Resour. Res.*, vol. 55, no. 11, pp. 8721–8739, 2019. doi: 10.1029/2018WR023758.

[312] R. E. Kennedy, Z. Yang, W. B. Cohen, E. Pfaff, J. Braaten, and P. Nelson, "Spatial and temporal patterns of forest disturbance and regrowth within the area of the Northwest Forest Plan," *Remote Sens. Environ.*, vol. 122, pp. 117–133, July 2012. doi: 10.1016/j.rse.2011.09.024.

[313] O. Viedma, J. Meliá, D. Segarra, and J. Garcia-Haro, "Modeling rates of ecosystem recovery after fires by using landsat TM data," *Remote Sens. Environ.*, vol. 61, no. 3, pp. 383–398, 1997. doi: 10.1016/S0034-4257(97)00048-5.

[314] A. Vrieling et al., "Vegetation phenology from Sentinel-2 and field cameras for a Dutch barrier island," *Remote Sens. Environ.*, vol. 215, pp. 517–529, Sept. 2018. doi: 10.1016/j.rse.2018.03.014.

[315] M.-D. Olivier, S. Robert, and F. Richard A, "A method to quantify canopy changes using multi-temporal terrestrial lidar data: Tree response to surrounding gaps," *Agric. For. Meteorol.*, vols. 237–238, pp. 184–195, May 2017. doi: 10.1016/j.agrformet.2017.02.016.

[316] Y. Ma et al., "Remote sensing big data computing: Challenges and opportunities," *Future Gener. Comput. Syst.*, vol. 51, pp. 47–60, Oct. 2015. doi: 10.1016/j.future.2014.10.029.

[317] Q. Guo et al., "Application of deep learning in ecological resource research: Theories, methods, and challenges," *Sci. Chin., Earth Sci.*, vol. 63, pp. 1457–1474, Mar. 2020. doi: 10.1007/s11430-019-9584-9.

[318] B. C. Bright, J. A. Hicke, and A. T. Hudak, "Estimating aboveground carbon stocks of a forest affected by mountain pine beetle in Idaho using lidar and multispectral imagery," *Remote Sens. Environ.*, vol. 124, pp. 270–281, Sept. 2012. doi: 10.1016/j.rse.2012.05.016.

[319] P. Tompalski, N. C. Coops, J. C. White, and M. A. Wulder, "Enhancing forest growth and yield predictions with airborne laser scanning data: Increasing spatial detail and optimizing yield curve selection through template matching," *Forests*, vol. 7, no. 12, p. 255, 2016. doi: 10.3390/f7110255.

GRS